A multi-instrumental approach for calibrating ~~two~~ real-time mass spectrometers using high performance liquid chromatography and positive matrix factorization

Melinda K. Schueneman[1], Douglas A. Day[1], Dongwook Kim[1], Pedro Campuzano-Jost[1], Seonsik Yun[1], Marla P. DeVault[1], Anna C. Ziola[1], Paul J. Ziemann[1], and Jose L. Jimenez[1]

[1]Department of Chemistry and Cooperative Institute for Research in Environmental Sciences, University of Colorado, Boulder, CO 80309, USA

Corresponding Author: Jose L. Jimenez, jose.jimenez@colorado.edu

Abstract. Obtaining quantitative information for molecular species present in aerosols from real-time mass spectrometers such as an extractive electrospray time-of-flight mass spectrometer (EESI) and an aerosol mass spectrometer (AMS) can be challenging. Typically, molecular species are calibrated directly through the use of pure standards. However, in some cases (e.g. secondary organic aerosol [SOA] formed from volatile organic compounds [VOCs]) direct calibrations are impossible, as many SOA species can either not be purchased as pure standards or have ambiguous molecular identities. In some cases, bulk~~from real-time soft-ionization aerosol instruments such as an Extractive Electrospray time-of-flight Mass Spectrometer (EESI) can be challenging, due to many individual species having different, and often hard to predict, sensitivities. Directly calibrating is time-consuming and relevant standards are often hard to obtain. In addition, the molecular identities of many of the sampled species may be ambiguous. Bulk~~ OA sensitivities are ~~sometimes~~ used to estimate molecular sensitivities. This approach is not sufficient for EESI, which measures molecular components of OA, because different species~~, but different types of OA~~ can have ~~bulk~~ sensitivities that vary by a factor of ~~~10.~~more than 30. Here, we introduce a method to obtain EESI calibration factors when standards are not available, and we provide a thorough analysis of the feasibility, performance, and limitations of this new technique. In this method, complex aerosol mixtures were separated with high performance liquid chromatography (HPLC) followed by aerosol formation via atomization. The separated aerosols were then measured by an EESI and an AMS, which allowed us to obtain sensitivities for some species present in standard and SOA mixtures. Pure compounds were used to test the method and characterize its uncertainties, and obtained sensitivities were consistent within ± 20 % when comparing direct calibrations vs HPLC calibrations for a pure standard, and within a factor of two for a standard mixture. In some cases, species were not completely resolved by chromatography, and positive matrix factorization (PMF) of AMS data enabled further separation. This method should be applicable to other real-time MS techniques. Improvements in chromatography are possible that would allow better separation in complex mixtures.~~A system to separate the compounds present in~~

~~complex samples can enable their direct calibration. Here, high performance liquid chromatography (HPLC) followed by aerosol formation via atomization was combined with online, 1 Hz measurements to calibrate the EESI and a High Resolution Aerosol Mass Spectrometer (AMS) for compounds present in a secondary organic aerosol (SOA) mixture. Pure compounds were used to test the method and characterize its uncertainties. Pure compound calibration factors were consistent within ±20% for direct atomization vs. HPLC separation, which is far superior to the orders of magnitude sensitivity differences that are possible with EESI. For species that were not well separated by chromatography, Positive Matrix Factorization (PMF) based on AMS spectra was used to test its ability to separate overlapping species. In two test cases, further separation was achieved using PMF, but derived sensitivities from direct and HPLC calibrations varied by up to a factor of 2.~~

TOC figure

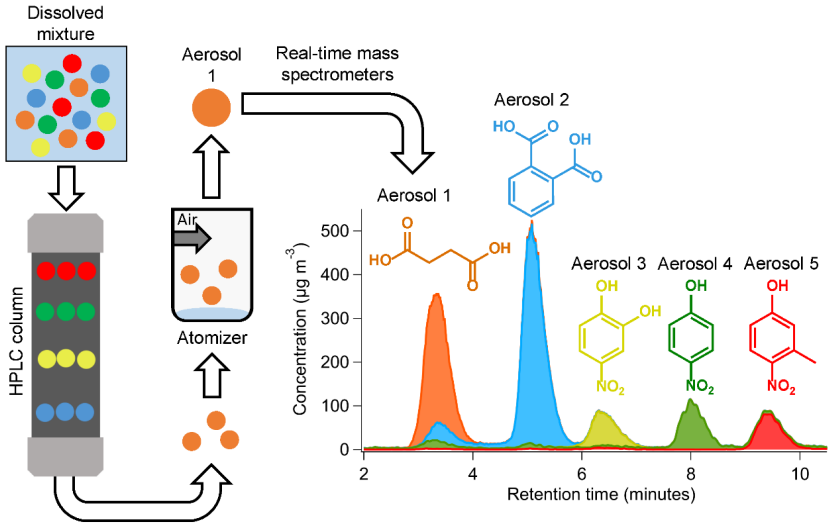

1 Introduction

Atmospheric aerosols are a complex, and often poorly understood, component of Earth's atmosphere. Aerosols have significant effects on both human and ecosystem health, and are significant contributors to anthropogenic climate forcing (Dockery et al., 1996; Lighty et al., 2000; Lohmann et al., 2004; IPCC, 2013). Organic aerosol (OA) is a substantial component of global aerosol levels (Kanakidou et al., 2005; Zhang et al., 2007; Jimenez et al., 2009). Since the early 2000s an important instrument for measuring OA concentrations in real -time has been the ~~Aerosol~~ aerosol ~~Mass~~ mass ~~Spectrometer~~ spectrometer (AMS) (Jayne et al., 2000; Canagaratna et al., 2007) and its high-resolution version (HR-AMS) (DeCarlo et al., 2006). Soft -ionization aerosol mass spectrometers, such as the ~~Extractive~~ extractive ~~Electrospray~~ electrospray ~~Time~~time-of-~~Flight~~ flight ~~Mass~~ mass ~~Spectrometer~~ spectrometer (EESI -ToF- MS, EESI hereinafter), have more recently become important tools for obtaining more detailed OA speciation (Lopez-Hilfiker et al., 2014, 2019; Eichler et al., 2015).

EESI can detect individual molecular ions (referred to henceforth as either molecular ions or individual species, even if they may comprise several isomers) from the particle -phase with 1 s time resolution (Lopez-Hilfiker et al., 2019; Pagonis et al., 2021). EESI has been used to measure aerosols in urban areas (Qi et al., 2019, 2020; Stefenelli et al., 2019; Kumar et al., 2022), in biomass burning (Qi et al., 2019; Pagonis et al., 2021), in cooking emissions (Qi et al., 2019; Brown et al., 2021), and for chamber studies of secondary OA (SOA) formation (Liu et al., 2019; Pospisilova et al., 2020). Many studies have illustrated the low detection limits, limited fragmentation, and other capabilities of the EESI; e.g. Lopez-Hilfiker et. al. (2019) and Pagonis et. al. (2021).

However, obtaining quantitative information for individual species from EESI measurements of complex mixtures of unknown species can be challenging~~,~~. This is due to each species having different~~,~~ and often hard to predict~~,~~ sensitivities (Law et al., 2010; Lopez-Hilfiker et al., 2019; Brown et al., 2021; Wang et al., 2021). In addition, EESI measures molecular ions, but can in some cases cause fragmentation, such as due to loss of HNO_3 from nitrates (Liu et al., 2019). For ~~an~~ SOA ~~mixture~~ from a single precursor, the bulk sensitivity compared to SOA formed from a different precursor has been shown to vary by a factor of 15 or more (Lopez-Hilfiker et al., 2019). Different studies also show that the bulk sensitivity for OA formed from different emission sources, (e.g. cooking, biomass burning,) can vary by a factor of ~ 10 (Qi et al., 2019; Stefenelli et al., 2019; Brown et al., 2021). For pure organic standards, the sensitivity can vary by a factor of 30 or more (Lopez-Hilfiker et al., 2019). Instead of directly measuring compound sensitivity, some groups use machine -learning (Liigand et al., 2020) or thermodynamic modeling (Kruve et al., 2014) to approximate instrument response factors for individual species. Other studies use bulk calibration factors for complex mixtures as an approximation for quantification (Tong et al., 2022).

Sensitivities can vary due to differences in analyte solubility (Law et al., 2010), EESI working fluid composition, sample composition, and different instrument conditions and settings, including polarity and changes in inlet pressure (Lopez-Hilfiker et al., 2019; Pagonis et al., 2021). Calibrating the EESI for individual species can be a challenging task, especially when standards are unavailable for most atmospheric oxidation products. In addition, OA from chamber experiments or field studies often contains unidentified molecular ions, or those whose species identity is ambiguous.

Several calibration methods have been applied to EESI. For example, direct calibrations were performed for many organic standards in Lopez-Hilfiker et. al. (2019), for 4-nitrocatechol (EESI~~(-)~~) and levoglucosan (EESI+) in Pagonis et al. (2021) to track sensitivity during each aircraft flight, and levoglucosan for regular sensitivity tracking during an indoor cooking study (and several other compounds less frequently and bracketing the campaign) in Brown et. al. (2021). During research field studies, often only one or two species are calibrated frequently, and the rest are quantified using relative response factors measured less frequently (Qi et al., 2019; Brown et al., 2021; Pagonis et al., 2021).

A recent ~~paper~~ study combined measurements from the Vocus Proton- Transfer Mass Spectrometer (Vocus), AMS, and EESI to measure speciated response factors without the need for standards. In that study, SOA was generated using an ~~Oxidation~~ oxidation ~~Flow~~ flow ~~Reactor~~ reactor (OFR). Following SOA formation, the Vocus measured the gas phase species, and the AMS and EESI measured the bulk and speciated particulate phase, respectively. EESI response factors were obtained through comparison to decreasing gas- phase mixing ratios measured by the Vocus as they condensed to the particle- phase (Wang et al., 2021).

Another method for obtaining calibration information is ~~Positive~~ positive ~~Matrix~~ matrix ~~Factorization~~ factorization (PMF). PMF is a type of factor analysis that allows approximate~~ly~~ apportioning of aerosol mass measured with online mass spectrometers and other instruments to atmospheric sources or level of oxidation (Zhang et al., 2005; Lanz et al., 2007; Ulbrich et al., 2009). To our knowledge, PMF has not been used with AMS data alone to obtain mass spectra and time series for individual molecular components. Separation with PMF alone ~~would~~ could be difficult for ambient or chamber experiment data~~, in part,~~ since most compounds likely co-vary in time and thus would not be statistically resolvable (Craven et al., 2012). Direct calibrations have been conducted to generate high- resolution AMS mass spectra for individual species (Ulbrich et al., 2019). A combination of AMS and PMF has been used to obtain quantitative information for EESI bulk measurements or PMF factors (Qi et al., 2019, 2020; Kumar et al., 2022). PMF has also been used on a combined data set consisting of both EESI and AMS data (Tong et al., 2022).

To our knowledge, PMF has not been applied previously to AMS and EESI chromatographically- separated data. Running PMF on chromatographic data may be able to generate species- specific mass spectra and time series for compounds that cannot be obtained ~~directly~~as pure standards. PMF has been applied in the past to gas chromatography mass spectrometry (GC- MS) data (Zhang et al., 2014, 2016; Gao et al., 2018), but not to ~~High~~ high ~~Performance~~ performance ~~Liquid~~ liquid ~~Chromatography~~ chromatography (HPLC) data, which is better suited for oxidized SOA species than GC, to our knowledge. AMS detection following HPLC separation has been conducted previously (Farmer et al., 2010) to explore AMS spectra of the separate compounds, but not for quantification. HPLC has not been previously combined with EESI or PMF, to our knowledge. Further, HPLC must be used here because the mass spectrometric detection needs to be much faster than the chromatographic time scale (on the order of seconds). Otherwise, this method is not applicable, and the different species separated by the chromatography would not be sufficiently resolved for speciated detection with the EESI and AMS.

Here, for the first time, we demonstrate a method combining ~~High Performance Liquid Chromatography~~ ~~(~~HPLC~~)~~, atomization, and detection by EESI, AMS, and s~~S~~canning ~~Mobility~~ mobility p~~P~~article s~~S~~izer (SMPS). The

method was validated by running pure standards, standard mixtures, and~~separating a mixture of standards, and then applied to~~ chamber SOA. The analyte peaks measured with each instrument were~~as~~ integrated, and calibration factors for separated species were calculated for the EESI (CF_x^E). The AMS response factor (CF_x^A, or RIE * CE, the product of the relative ionization efficiency and collection efficiency) and the atomic oxygen to carbon (O:C) ratio for different analytes were quantified. EESI calibration factors (CF_x^E) for individual compounds were determined and compared to literature values. In cases where ~~full peak separation via~~ HPLC ~~alone was not achieved~~did not fully resolve all analytes, PMF was run on the ~~EESI and~~ AMS mass spectral matrices to obtain further compound separation.

2 Methods

2.1 Chamber experiments and filter mass collection

SOA was generated using the procedure of DeVault et. al. (2022). Briefly, chamber experiments were conducted in a ~~6.9 (±0.5)~~ n 8.0 m^3 T~~t~~eflon chamber (Claflin and Ziemann, 2018; Bakker-Arkema and Ziemann, 2021)~~(Bakker-Arkema and Ziemann, 2021)~~. The temperature (23 °C) and atmospheric pressure (0.83 atm) were constant. Ammonium sulfate seed was added to ~~a~~ the humidified chamber (RH = 55 %), followed by β-pinene, which was evaporated from a heated glass bulb. In the dark, N_2O_5 was added as the NO_3 source, from the sublimation of cryogenically- trapped solid N_2O_5. During these experiments, ~ 372 - 1378 µg m^{-3} SOA was made within the large reaction chamber. This material was collected on a filter for ~ 120 min at a flow rate of 14 L min^{-1}. Following dissolution in solvent, ~ 16 - 56 µg of SOA was injected into the HPLC. Further discussion is included in Sect. S4. The experiment was modeled after Claflin et. al. (2018).

Following SOA formation, a 0.45 µm Millipore Fluoropore PTFE filter was used to collect SOA. The combined filter and ~~+~~aerosol was~~was~~ weighed after aerosol collection. The combined filter and ~~+~~aerosol was exposed to minimal ambient air, and was always handled with artificial lighting turned off and outdoor blinds drawn. After weighing, each filter was extracted in 2 mL of HPLC grade ethyl acetate (EtAc) twice. The 4 mL aerosol extract/EtAc mixture was dried using pure N_2. Once the EtAc was evaporated, the leftover material was dissolved in HPLC grade acetonitrile (ACN) and stored in a freezer at - 23 °C (DeVault et al., 2022). The extract used here was the same as DeVault et. al. (2022), and was ~~one~~ 1 year old at the time of analysis. ~~That study showed that the~~DeVault et al. (2022) showed that this SOA is composed entirely of acetal dimers, which are exceptionally stable~~,~~. Therefore, ~~so~~ the SOA is unlikely to have changed significantly over this period.

2.2 High Performance Liquid Chromatography (HPLC)

HPLC separation was performed using a Shimadzu Prominence HPLC, coupled to a Zorbax Eclipse XDB-C18 column (250 × 4.6 mm with 5 µm particle size). A Nexera X2 SPDM30A UV / vis photodiode array detector was used to generate absorbance chromatograms. The column stationary phase was designed for reverse mode, where smaller, more polar species had shorter elution times. Separated species were measured first at **λ** = 210 nm and **λ** = 254 nm using an UV-Vis diode array detector with a reference wavelength of 300 nm. Separated chemical components then flowed into a high- flow Collison atomizer, forming droplets and then aerosols consisting solely of the SOA compounds after evaporating the HPLC solvent in a Nafion drier. The aerosols were then measured by a suite of instruments, shown in Fig. 1, and pictured in Fig. S1. Tubing delay times are also included in Table S1.

Field Code Changed

Formatted: Superscript

Formatted: Superscript

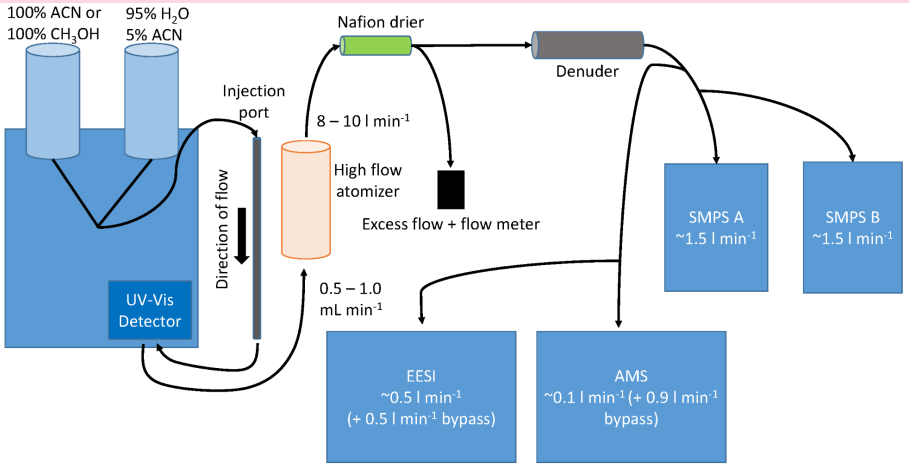

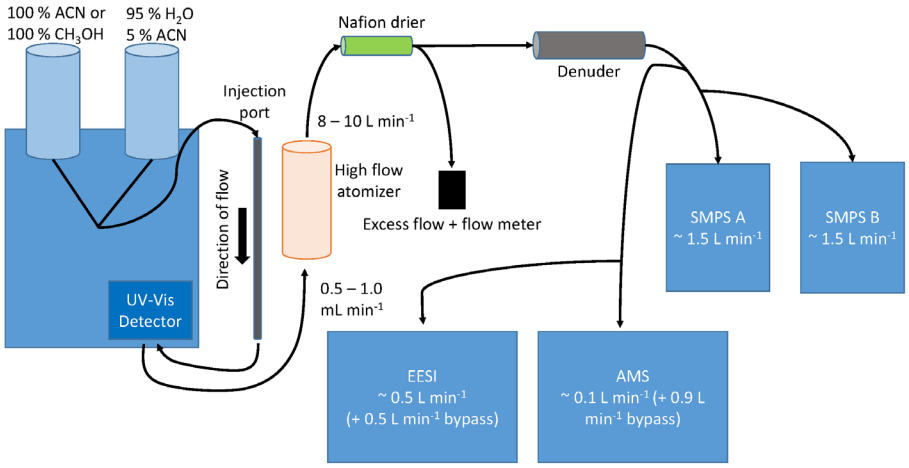

Figure 1. HPLC schematic. Left, HPLC containing a column and a UV-Vis detector. Following separation, the column effluent was sent to an atomizer, dried, and the aerosol was detected by each of the instruments shown.

A maximum volume of 50 µL ACN / aerosol mixture was injected into the column at once. At the beginning of each day, the HPLC solvent lines (HPLC grade acetonitrile and HPLC grade water) were flushed to remove any air bubbles that may affect elution. Following this, a clean cycle was run by injecting 50 µL HPLC grade ACN into the reverse- phase column. This ensured previous HPLC run species did not contaminate new runs. The first run of the

Commented [P1]: Delete image, new image has correct formatting

day, post cleaning cycle, was a 4-nitrocatechol / 4-nitrophenol mixture (dissolved in ACN). These species were well characterized by the particle- phase instruments and have measurable absorbances at the recorded UV wavelengths.

For each experiment, the mobile phase consisted either of an ACN / water mixture or an ACN / CH_3OH / water mixture. The mixture varied in relative concentrations of each solvent over the course of each HPLC run. Most experiments were started at 95 % water / 5 % ACN (solvent mixture A). The mobile phase became less polar over time. For some systems, solvent B (pure acetonitrile) replaced solvent system A as time went on. For other systems, solvent C (pure methanol) was used. Each standard and / or SOA system was run under different conditions, depending on the separability of different components.

For the standard solution run, a mixture of solvent A and solvent B was used. Using a flow of 1.0 mL min^{-1}, solvent B was increased from 0 % to 35 % in 1 ~~minute~~min, then 35 % - 40 % for 5 min~~utes~~, followed by 40 % - 50 % for 3 min~~utes~~, and 50 % - 100 % for 2 min~~utes~~, this is also shown in Fig. S2a. For the β-pinene SOA extract, the flow rate was set to 0.5 mL min^{-1}, and a mobile phase gradient started at 20 % solvent C for 2 min~~utes~~, then increased at a rate of 6 % min^{-1} up to solvent C of 50 %, followed by an increase of 3 % min^{-1} to a concentration of 80 % solvent C, then 0.75 % min^{-1} until 95 % solvent C, held at 95 % C for 20 min~~utes~~ and increased by 1.7 % min^{-1} to 100 %, following 10 min~~utes~~ at 100 % solvent B, shown in Fig. S2b (DeVault et al., 2022).

2.3 Standards for HPLC measurements

Two standard solutions of atmospherically relevant species were made for this study. Standard solution 1 contained 0.4 % (by mass) 3-methyl-4-nitrophenol, 0.2 % phthalic acid, 0.5 % 4-nitrophenol, 0.6 % succinic acid, and 0.1 % 4-nitrocatechol, dissolved in HPLC grade acetonitrile. Solution 2 contained 8 species: 0.3 % phthalic acid (by mass), 0.3 % L-malic acid, 0.1 % succinic acid, 0.3 % citric acid, 0.3 % levoglucosan, and 0.2 % 4-nitrocatechol in HPLC grade acetonitrile. Source information and calculated saturation mass concentrations for all species are shown in Table S2.

Each species was chosen for its relevance in biomass, urban, or manufacturing processes. 3-methyl-4-nitrophenol, 4-nitrophenol, 4-nitrocatechol and levoglucosan are cyclic C_6 carbon species found in biomass burning. Succinic acid, L-malic acid, and phthalic acid are ~~non-cyclic~~ acids of secondary origin found in urban atmospheres. Citric acid is found in food and / or medicine. A critical property of these compounds is that they absorb in the UV-Vis, whereas most SOA does not. Nitrates and aromatics have strong absorbance and carboxylic acids have a very weak absorbance.

2.4 Aerosol Generation and Sampling System

The HPLC was coupled to particle phase measurements by using a high- flow Collison atomizer. First, a ~~t~~Teflon line was attached to the waste port of the HPLC. The flow from the HPLC was 0.5 - 1 mL min^{-1}, all of which was sent to the atomizer. The atomizer operated by first introducing pressurized compressed air (~ 20 psi) into a small chamber (473 ~~ml~~ mL jar). Perpendicular, sample flow at a rate of 0.5 or 1 mL min^{-1} intersected the pressurized air. This led to the generation of particles of a consistent size distribution, and provided a total flow ranging from 8 to 10 L~~l~~ min^{-1}. Instrument specific flows were measured daily.

Following atomization, ~ 10 ~~l~~ L min^{-1} of aerosol / solvent flow was sent through a Nafion dryer before being sent through an activated carbon denuder. This denuder is in a stainless steel, ~ 1 inch diameter and 8 inch length tube, composed of activated carbon honeycomb cross- sections. Flow was then sent into each particle instrument. Solvent was efficiently removed (> 99.0 %, Pagonis et. al. (2021)) using the carbon denuder. Acetonitrile (a solvent used in the HPLC system) was monitored using the EESI. ~~If acetonitrile started to increase, the EESI denuder was regenerated.~~ Denuder regeneration was typically only necessary after the first 4 h of each experiment.

Residence times in different parts of the system were estimated to enable synchronizing the aerosol instrument observations ~~with~~ and the measured UV-Vis absorbances. Calculations shown in Table S1 suggest that a delay of at least ~~41~~ 40 ~~seconds~~ should be observed between the UV-Vis measurement and detection with the aerosol instruments, which is consistent with the measured delay. Retention times for EESI, AMS, and SMPS may differ from each other by 1 - 2 ~~seconds~~, depending on the residence times in the tubing. In addition, bypass flows (shown in Fig. 1) were added to the EESI and AMS to reduce residence times in the tubing and thus particle losses or evaporation. These delay differences were handled by shifting instrument data by the delay times.

2.5 Description of particle measurements

2.5.1 Extractive Electrospray Time- of- Flight Mass Spectrometry (EESI)

The EESI uses a soft ionization technique that detects particle- phase analytes based on their solubility and proton affinity / adduct formation stability (Lopez-Hilfiker et al., 2019). Briefly, particle / gas sample flow was sent into the EESI source at ~0.5 - 1 ~~l~~L min^{-1}, where gases are removed using a charcoal denuder (> 99 % removal efficiency for acetic acid, when regenerated daily) (Tennison, 1998; Pagonis et al., 2021). The aerosol inlet for the instrument used in this study was pressure controlled (Pagonis et al., 2021), and was run at ~~766~~ 575 mbar. While designed for aircraft applications, the pressure- controlled inlet provides better spray and signal stability as it shields the spray from small pressure perturbations from changes in upstream inlet flow conditions. This includes perturbations caused by ~~such as~~ switching between different sampling modes and plumbing pathways. ~~The~~ Here, the working fluid consisted of a mixture of 25 % milli-Q water and 75 % (by volume) HPLC grade methanol. The EESI was run in two polarity modes. The positive polarity mode (henceforth "EESI+") contained 200 ppm of sodium iodide (NaI) (Pagonis et al., 2021). This working fluid generally forms Analyte-Na^+ adducts. The negative polarity mode (EESI-) was doped with 0.1 % (by volume) formic acid (Chen et al., 2006; Gallimore and Kalberer, 2013; Pagonis et al., 2021). Species with a lower proton affinity than formate donate a proton and become negatively charged. This ionization mode is generally sensitive to acidic species that can readily donate a proton and become anionic.

For both polarities, a fused silica capillary (TSP Standard FS tubing, 50 µm ID, 363 µm OD) was used to transport working fluid solution from a pressurized (250 - 300 mbar above ambient) fluid bottle. Typical resolution at *m/z* 150 was 4000, and mass spectra were saved every second.

The mass concentration of a species (µg m^{-3}) can be quantified from its EESI signal (I_x ion counts s^{-1}) as (Lopez-Hilfiker et al., 2019):

$$Mass_x = I_x(\frac{MW_x}{RF_x}) \cdot \frac{1}{F} \quad (1)$$

MW_x is the molecular weight of species x, F is the flow rate (in L min^{-1}), and RF_x is the combined response factor. There are ~~representing~~ fundamental parameters for EESI signal which ~~can be found~~are described further in Lopez-Hilfiker et. al. (2019). Here, we define a new variable, EESI calibration factor (CF_x^E, in µg m^{-3} counts^{-1} s), such that

$$Mass_x = I_x \cdot CF_x^E \quad (2)$$

Generally, CF_x^E is directly determined by direct calibrations with standards, when possible. Here, CF_x^E was determined by either direct calibrations using either commercially available standards or HPLC-separated analytes. Calibration factors are reported as absolute values (in units of counts s^{-1} µg^{-1} m^3) and also relative to 4-nitrocatechol for EESI- and levoglucosan for EESI+ (unitless).

2.5.2 High Resolution Aerosol Mass Spectrometer (HR-AMS)

A high-resolution time-of-flight aerosol mass spectrometer (hereinafter AMS) (DeCarlo et al., 2006; Canagaratna et al., 2007) was used to obtain 1 Hz chemical composition for organic aerosol (OA) and nitrate aerosol (pNO_3). The AMS was run with an inlet flow of 0.1 L~~l~~ min^{-1}, and a bypass flow of ~ 1.3~~ 4 L~~l~~ min^{-1}. The AMS was run exclusively in "fast mode" (Kimmel et al., 2011; Nault et al., 2018), and size distributions were not recorded. AMS backgrounds were measured for 6 s~~econds~~ every 52 s~~econds~~. Outside of HPLC runs, the AMS background was < 0.1 µg m^{-3}. Between eluting peaks A~~a~~dditional backgrounds were taken~~, in part~~ to test for solvent residue and / or residual influence from ~~the~~ previous HPLC runs.~~, were taken during the times where no peaks were eluting, and~~ These backgrounds were generally ~~remained~~ < 2 µg m^{-3} for both the AMS and the SMPSs. The detection limit (DL) and limit of quantification between eluting peaks was 0.7 µg m^{-3} and 2.2 µg m^{-3}, respectively, suggesting that background subtracted concentrations above 2.2 µg m^{-3} can be accurately measured. The latter were conducted by flowing the sampler air through a particle filter. AMS data was analyzed in the ToF-AMS analysis software (PIKA version = 1.25F, Squirrel = 1.65F) (DeCarlo et al., 2006; Sueper, 2023) within Igor Pro 8 (Wavemetrics, Lake Oswego, OR). ~~The~~ When AMS sensitivities were not obtained from direct measurements, the AMS OA relative ionization efficiency (RIE) and collection efficiency (CE) were assumed to be 1.4 ($OA_{default}$, (Canagaratna et al., 2007)) and 1, respectively. The AMS NO_3 RIE * CE ($NO_{3,\ default}$) was assumed to be 1.1 (Canagaratna et al., 2007). Data herein is reported in µg m^{-3}, using Boulder pressure (P = 830 mbar) and average lab temperatures (~ 20 °C).

Here, the quantification of different particle-phase species that have been separated by HPLC (and thus are mostly in single component particles) is assessed for the AMS. This is a function of RIE_X * CE_X (a.k.a. "AMS response factor", or CF_x^A) for a species X. Direct AMS calibration has been reported for many OA species (Slowik et al., 2004; Dzepina et al., 2007; Jimenez et al., 2016; Xu et al., 2018; Nault et al., 2023). An RIE of 1.4 is typically applied to ambient organic aerosols (Canagaratna et al., 2007), which has been shown to perform well in most outdoor intercomparisons (Jimenez et al., 2016; Guo et al., 2021). Laboratory measurements typically require

Formatted: Superscript

Formatted: Superscript

Formatted: Superscript

specific calibrations, as RIE can be higher for some compounds and mixtures (Jimenez et al., 2016; Xu et al., 2018; Nault et al., 2023). CE can vary considerably, from CE = 0.15 to a CE = 1 (Docherty et al., 2013).

The material densities of the known standards were determined by running the AMS in PToF mode and calculating the density as d_{va} / d_m ~~(~~, where d_{va} is the aerodynamic vacuum diameter~~,~~ and d_m is the SMPS measured mobility diameter (DeCarlo et al., 2004)~~)~~. Calculated densities are shown in table S2. For the unknown species present in the SOA, densities were estimated using the atomic ratio of oxygen plus nitrogen to carbon ([O+N]:C) and H:C, as demonstrated in Day et. al. (Day et al., 2022), which builds upon the method of Kuwata et. al. (Kuwata et al., 2012) which did not account for nitrate content. The O:C ratio attributed to the non-nitrate OA was calculated per Canagaratna et. al. (2015). The organic nitrate contribution was quantified per Day et. al. (2022). All nitrate here was assumed to be from organic nitrate functional groups, as the aerosol studied here likely contained little inorganic nitrate. For the density calculation, the total nitrate was multiplied by the ratio of the molecular weights of NO_2:NO_3 (46 / 62) and converted into a molar concentration using the molecular weight of NO_2 (46 g mol^{-1}). Only the NO_2 functionality was included for the density calculation, since the nitrate oxygen bonded to the carbon is expected to typically be included as part of the standard AMS OA O:C estimation (Farmer et al., 2010). Carbon was also converted into a molar concentration using the molecular weight (12 g mol^{-1}). That organic nitrogen to organic carbon ratio was added to the standard AMS OA O:C ratio to obtain the organic nitrate~~-~~ corrected [O+N]:C ratio.

For isolated peaks that contained organic nitrate, the organic nitrate (NO_3) concentration was added to the AMS OA to get the total measured AMS mass. The SMPS mass was then compared to the AMS mass calculated with the default CF_x^A, and the correct CF_x^A was determined with Eq. 3 (further details in Sect. 2.7).

$$CF_x^A = \frac{OA\ default + NO_{3,default}}{SMPS\ mass} \quad (3)$$

For HPLC peaks composed of multiple species (like in the β-pinene SOA sample), the average CF_x^A was calculated by adding the average NO_3 contribution (~ 5 %) to the measured AMS OA contribution (Fig. S3). This CF_x^A was then applied to the AMS PMF organic chromatographic time series, in order to determine CF_x^E. For species not containing any nitrate, the $NO_{3,\ default}$ was set to 0.

We note that some recent work has suggested that the sensitivity of organic nitrate functional groups may be lower than for ammonium nitrate (for which the nitrate is calibrated by default in AMS data processing). Thus, a correction of ~ 62 / 46 may be more appropriate here for computing nitrate functional group mass concentrations (Takeuchi et al., 2021). However, due to the small nitrate contribution overall, such a correction ~~is~~ was not applied.

2.5.3 Scanning Mobility Particle Sizer (SMPS)

Two SMPSs were run with a 20 s~~econd~~ offset during HPLC experiments (consisting of all TSI, Inc components) in order to improve the time resolution of the total particle volume measurement. For both SMPSs, a 3081 differential mobility analyzer (DMA) was run with a 3080 ~~Electrostatic~~ electrostatic c~~C~~lassifier. Each was coupled with either a 3776 condensation particle counter (CPC) (referred to as SMPS A) or a 3775 CPC (SMPS B). Both systems were run in the CPC "high flow" mode. Sample flow rates were nominally set to 1.5 ~~l~~L min^{-1}, but the actual (measured

flow) was 1.43 and 1.49 ~~l~~L min^{-1} for the 3776 and 3775, respectively. DMA sheath flows were set to 6.0 ~~l~~L min^{-1}. Data were compared to that acquired in a reference mode, with a sample flow of 0.3 ~~l~~L min^{-1}, a sheath flow of 3.0 ~~l~~ L min^{-1}, and 120 s scans. Testing was done to ensure that number and volume distributions and integrated concentrations matched between the reference and fast scanning modes, shown in Fig. S4 and discussed in depth in Sect. S3. The SMPSs were also run concurrently during an HPLC run to confirm that data from both instruments matched (Fig. S5). Overall, the SMPSs in the reference and fast modes agreed within 10 %. Flows were measured every day, and delay times (from the SMPS inlet to the CPC detection, which affect sizing) were calculated when changes in plumbing were made. Further details on SMPS delays can be found in Table S3.

2.5.4 Direct Calibration Procedure

Direct calibration refers to the standard method of generating monodisperse aerosol from a calibrant solution with a Collison atomizer (TSI model 3076) drying with a Nafion dryer, size selecting at 275 nm with a TSI 3080 electrostatic classifier / 3081 DMA, removing double charged particles with an impactor, measuring the particle concentration with a 3775 CPC, and measuring with the EESI and / or AMS. The EESI and AMS sensitivities were obtained by comparing their signals to the particle mass calculated from the known particle volume, estimated density, and CPC particle concentration.

Formatted: Space Before: 12 pt, After: 12 pt

Formatted: Font: Bold

2.6 Positive Matrix Factorization (PMF)

Positive Matrix Factorization (PMF) (Paatero and Tapper, 1994; Paatero, 1997) is a bilinear deconvolution model that relies on the assumption of mass balance with components with constant spectral profiles. Briefly, time series for signals at individual *m/z*'s are entered into a two-dimensional matrix with *m* rows (points in time) and *n* columns (*m/z*'s) (Ulbrich et al., 2009; Kumar et al., 2022). PMF works to minimize the squared weighted residuals between the measured and reconstructed matrices, producing multiple potential solutions that could explain different chemical or physical sources in a given data set, along with the total residual of each solution.

The model is solved using PMF2 (Paatero, 2007) and the multilinear engine, developed by Paatero et. al. (1999), run from the PMF Evaluation tool ("PET") software v3.08 in Igor Pro v8 (Wavemetrics, Lake Oswego, OR). Choosing the best PMF solution always has a subjective component, as it is usually impossible to know the "correct" number of factors that completely capture a complex data-set (Ulbrich et al., 2009). Several methods can be used to assess the validity of a given solution. First, the Q-value (Q), which is the total sum of the error-weighed square residuals for a data set, is used. Q_{exp} is the expected value of Q if all residuals are due to random errors with the estimated precision at each point. If the individual data points in a solution are fit so that the residuals are consistent with random noise, then $Q / Q_{exp} \sim 1$. Note that this also requires accurate estimation of the precision (random error) in the entire data matrix. In some situations, PMF cannot explain a data set within an acceptable error. In these situations, $Q / Q_{exp} >> 1$. All solutions here have $Q / Q_{exp} \leq 1$.

The second criteria for picking the best PMF solution is by exploring the time series and mass spectra for a given solution for different approximate rotations (FPEAK values) (Lee et al., 1999; Lanz et al., 2007; Ulbrich et al., 2009). Simply, PMF rotations are non-unique solutions that are represented across multiple factors. In a real-world

example, a source profile (for example, biomass burning OA), might split across multiple PMF factor's time series and/or mass spectra, despite only being from a singular source. Factor splitting can sometimes reduce residuals, and mathematically may appear as a more correct solution for a particular dataset. This is where the user must thoroughly assess different solutions, specifically those with $Q / Q_{exp} \leq \sim < \sim 1$.

PMF solutions chosen here are based on the above criteria and a third: the time series of the residuals. In a chromatogram, the shape of the peaks ~~are~~is generally known. Here, ~~4~~ four different instruments generate unique chromatograms: UV-Vis, ~~HR~~AMS, EESI, and the SMPSs. Thus, across those four instruments, the shape of the chromatogram was fairly well constrained. When choosing solutions here, the shape of the chromatogram was compared to the time series of the residuals. If the residuals showed significant peaks, then that was an indicator that not enough factors were used to represent the complete chromatogram and all of the factors therein.

The $m \times$ ~~x~~ n matrix for AMS data was generated for HR ions using the PMF export option in the PIKA data analysis software. Briefly, unit mass and high resolution AMS data were first fit as described in Sect. 2.5.2. After confirming that all ions of interest were well fit, the organic data was exported into an $m \times$ ~~x~~ n matrix (both signal and precision matrices). Any HR ions not associated with the following families: C_x, CH, CHO_1, and CHO_{gt1} were removed, as NO_3 was not included in the PMF input, and the included families were the only measured ions with substantial signal during the experiments included here. PMF was run from 1 - 20 factors. Rotations (FPEAKS) were enabled, ranging from - 1.0 to 1.0, in steps of 0.2.

2.7 Calculating calibration factors for species using the multi-instrumental method

For unknown species (or known species with an unknown AMS response factor) the following method was used to obtain EESI and AMS calibration factors:

1. Calculation of composition- dependent density using the measured elemental composition or d_{va} / d_m measured densities from AMS and SMPS data.
2. SMPS size distributions are fit with a lognormal curve, and integrated volume concentrations are obtained.
3. SMPS integrated volume time series were multiplied by the density, to produce the reference mass concentration time series.
4. The high- time- resolution AMS OA and NO_3 time series are obtained for an assumed RIE * CE = 1.4 ($OA_{default}$) and RIE * CE = 1.1 ($NO_{3,\ default}$).
5. The SMPS mass concentration time series and the AMS OA+NO_3 time series, for an individual chromatographic peak, are fit with a Gaussian distribution
6. The AMS and SMPS Gaussian distributions are integrated (µg m^{-3} s).
7. The CF_x^A was obtained using the ratio of the integrated SMPS to the integrated AMS time series fits (Eq. 3).
8. The time series for the EESI *m/z* was fit with a Gaussian and integrated along the retention time.
9. The integrated Ggaussian for the EESI *m/z* was divided by the integrated AMS (OA+NO_3, after AMS calibration by the SMPS) or SMPS ~~gaussians~~ Gaussians to obtain CF_x^E (counts s^{-1} m^3 μg^{-1}).

In step 9, the SMPS was used as the EESI reference for calculating CF_x^E when the analytes were resolved from chromatography alone. As discussed for the mixtures shown in Sect. 3.1, 3.2, and 3.3, we never obtained complete chromatographic separation. In cases of overlapping analytes, the SMPS used here does not have the time resolution to be used as the EESI reference. Instead, we referenced the EESI to the AMS by first calibrating the total AMS signal to the total SMPS signal for mixed peaks. We then used PMF results for the corrected AMS data and compared individual AMS PMF factors time series to EESI time series to calculate CF_x^E.

3 Results

3.1 Mass Balance of the Analyte in the Experimental System

There was substantial plumbing between the injected sample and the instruments measuring the analyte, where losses can occur (Fig. 1, Table S1). ~~In order t~~To better understand the experimental system, the mass flux was calculated using the known, injected mass as well as the tubing diameters, lengths, and flow rates, as shown in Fig. 2.

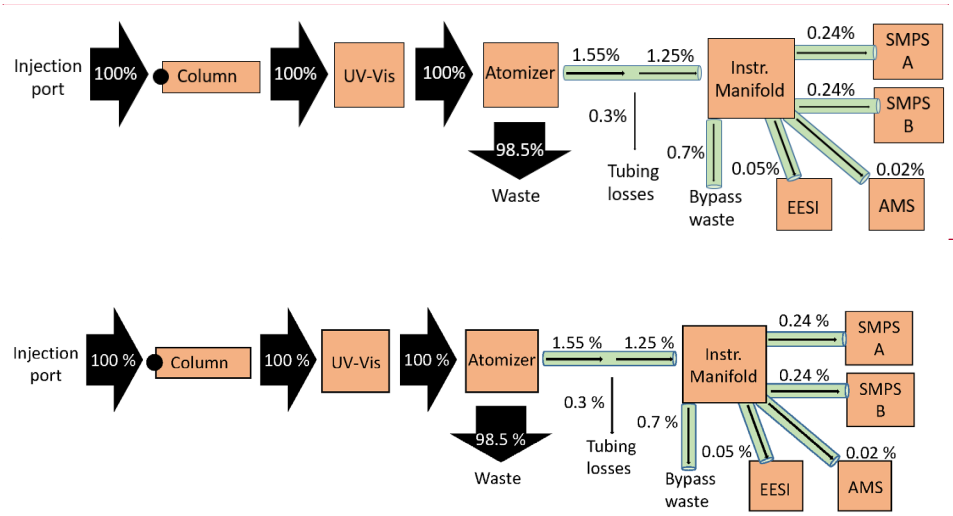

Figure 2. Mass flux across the multi-instrumental setup. Arrows are sized by the percentage of analyte mass, which is included alongside each arrow. EESI and AMS have bypass lines (represented as the total by 0.7 % bypass waste). Percentages shown are for the actual measured mass percent. Tubing details are also included in Fig. 1.

~~By i~~Injecting a known amount of sample into the HPLC column~~, we were able to account for~~ allowed us to track all the measured mass by the four instruments sampling. As shown in Fig. 2, all of the injected mass was analyzed by the UV-Vis spectrometer, but only a small fraction of it was analyzed (0.55 %) by the online instruments. There was substantial fluid loss at the atomizer, which is thought to account for the bulk of the mass leaving the HPLC. The EESI and AMS measure the least mass, due to their low flow rates (0.28~~ l~~ L min^{-1} and 0.1 ~~l~~L min^{-1}, respectively). Of the mass that exited the atomizer, ~ 20 % was lost in the tubing (~ 10 m, ¼" I~~.~~D~~.~~) to the aerosol sampling manifold (represented as 0.3 % of total in Fig. 2). Overall, the efficiency in sampling the injected mass with the online instruments was very low with this system, primarily due to the atomization process. In SOA extracts that are highly concentrated, this is not a major problem. However, application of this method to lower concentration samples would benefit from use of a lower- flow liquid chromatography method and a more efficient atomizer.

Commented [P2]: Delete image, new image w/ correct formatting

3.2 Application of multi-instrumental method and PMF for standard species' calibrations

3.2.1 Cross comparison between directly calibrated one- component chromatographic standards vs. multi-instrumental method

In order to test the efficacy of the proposed method, two solutions were made containing one standard each ~~(~~, either phthalic acid ~~and~~ or 4-nitrocatechol~~)~~. These species were first calibrated directly in order to obtain CF_x^E and CF_x^A, as described in Sect. 2.5.4. ~~Direct calibration hereout refers to the standard method of generating monodisperse aerosol from a calibrant solution with a Collison atomizer (TSI model 3076) drying with a Nafion dryer, size selecting at 275 nm with a 3080 electrostatic classifier / 3081 DMA, removing double-charged particles with an impactor, measuring the particle concentration with a 3775 CPC, and measuring with the EESI and/or AMS.~~ Then, each solution was injected into the HPLC to generate isolated chromatograms (Fig. 3).

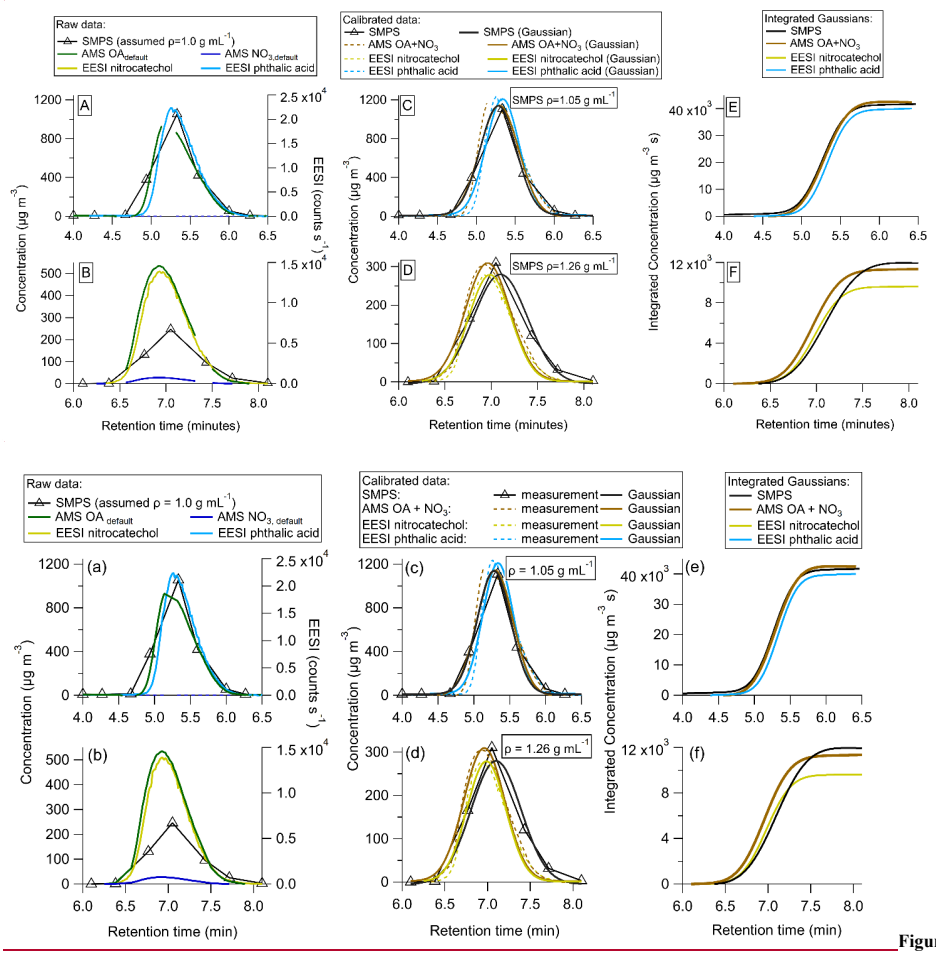

Figure 3. Single standard calibrations for (Aa) Uuncalibrated data collected during a single standard (HPLC data for phthalic acid) HPLC run, (Bb) raw data from a nitrocatechol HPLC rununcalibrated HPLC data for 4-nitrocatechol, (Cc) calibrated phthalic acid data (using the monodisperse calibration factors) HPLC phthalic acid data calibrated using the sensitivity derived from the direct calibration, (Dd) HPLC 4-nitrocatechol data calibrated using the sensitivity derived from the direct calibrationcalibrated nitrocatechol data, (Ee) integrated Gaussian peaks from (Cc), and (fF) integrated Gaussian peaks from (dD).

In Fig. 3a, the uncalibrated background- subtracted data is shown. Phthalic acid contains no nitrate moiety, so AMS NO_3 was 0. Fig. 3b shows the raw data for 4-nitrocatechol. Due to the nitro group, AMS NO_3 is added to AMS OA to obtain the total mass measured by the AMS. If the method was followed as described in Sect. 2.7, the raw data

Commented [P3]: Deleted, fixed formatting

would be fit with Gaussian curves and integrated, in order to produce CF_x^E and CF_x^A for each species. However, in this test study, CF_x^E and CF_x^A are already known through direct calibrations discussed in Sect. 2.5.4.

Figure 3c shows the HPLC phthalic acid peak with the direct calibration factor applied.~~directly calibrated (as opposed to the multi-instrumental approach calibrated) data for phthalic acid.~~ It is clear that the AMS, EESI, and SMPS data line up well, indicating that the multi-instrumental approach produces very similar CF_x^E and CF_x^A as the direct calibrations. Fig. 3d echoes this, showing good overlap across each instrument for 4-nitrocatechol.

Figures 3e and 3f show the integrated, calibrated Gaussian curves. If the multi-instrumental method worked as well as direct calibrations, the maximum integrated values would be expected to be the same for each instrument. For phthalic acid, the instruments agree within 6 %, with the EESI showing the largest deviation from the other instruments. For 4-nitrocatechol, this difference is 20 %, and again the EESI is the farthest from the other instruments. Such discrepancies could be due to changes in EESI sensitivity, which may be driven by the different solvents used for calibration (water for direct calibrations, and a mixture of acetonitrile and water for the multi-instrumental method). It could also be due to the high concentrations of each solute, which may change CF_x^E slightly.

Following method validation through comparison between direct calibrations and the multi-instrumental calibration method, a mixture containing five standards (phthalic acid, 4-nitrocatechol, succinic acid, 4-nitrophenol, and 3-methyl-4-nitrophenol) was run through the HPLC column (Fig. 4). Like above, each species was first calibrated directly, in order to compare the direct calibration values vs. the multi-instrumental calibration method for a more complex chemical system.

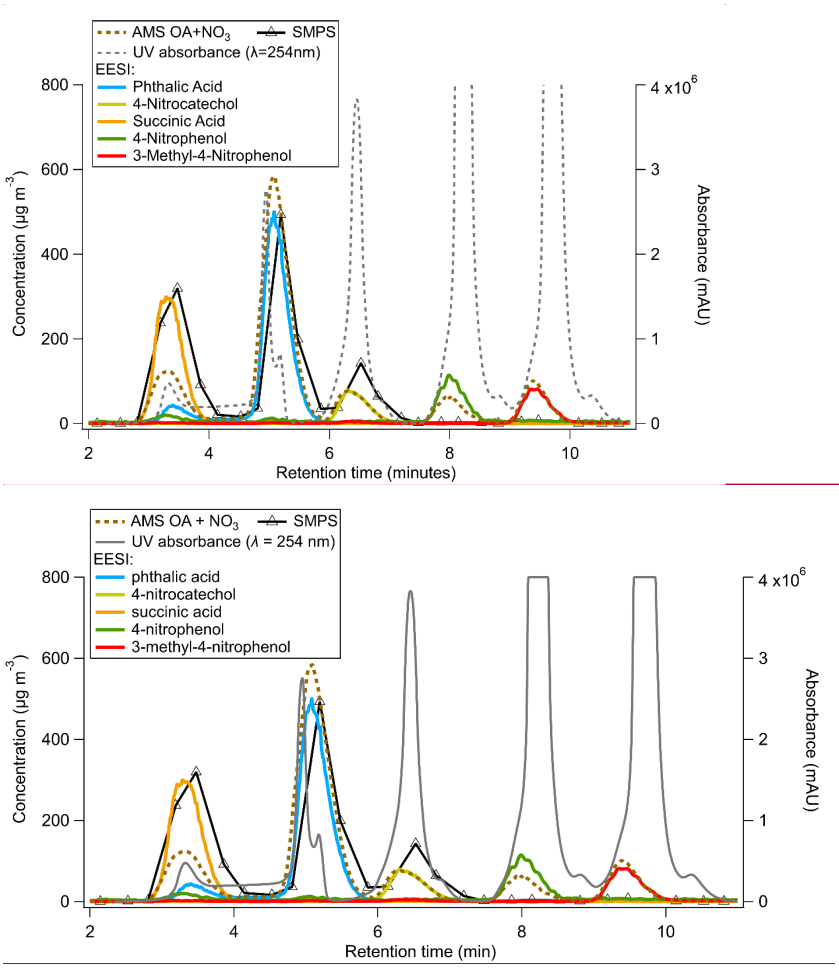

Figure 4. Time series of UV absorbance (milli-absorbance units) and AMS, EESI, and SMPS mass concentrations for a mixed-solution standard HPLC run.

In Fig. 4, succinic acid was the first peak to elute from the HPLC column, from ~2.5–4.0 minutes. The EESI and SMPS data match well, but the AMS data is lower by a factor of ~2. This is potentially driven by the phthalic acid/succinic acid co-elution (as evidenced by the EESI). The CF_x^A for both species is shown in Table 1. CF_x^A differ substantially, and an internal mixture of aerosols containing succinic acid and phthalic acid may result in a larger AMS bias (as $CF^A_{Succinic\ Acid}$ and $CF^A_{Phthalic\ Acid}$ differ significantly) than the EESI (where we measured molecular ions) or the SMPS (as the density of phthalic acid and succinic acid are similar, table S2).

Commented [P4]: Delete image, reformat

456

Table 1. Calibration factors for resolved (or mostly resolved) standard species. CF_x^E values are reported in counts s^{-1} μg^{-1} m^3 and the relative EESI calibrations factors (CF_x^E / CF_{nitro}^E (EESI-) or CF_x^E / CF_{levo}^E (EESI+)), and the AMS calibration factors (CF_x^A)are unitless values.

Species	Direct calibration CF_x^E (counts s^{-1} μg^{-1} m^3)	Multi- instr. calibration CF_x^E (counts s^{-1} μg^{-1} m^3)	Direct calibration CF_x^E / CF_{nitro}^E (EESI-) or CF_x^E / CF_{levo}^E (EESI+)	Multi- instr. calibration CF_x^E / CF_{nitro}^E (EESI-) or CF_x^E / CF_{levo}^E (EESI+)	Direct calibration CF_x^A (unitless)	Multi-instr. CF_x^A (unitless)
4-nitrocatechol (EESI-)	44~~.1~~ ± 5.0	23	1.0	1	~~1.96~~2.0 ± 0.17	1.0~~5~~1
4-nitrocatechol (EESI+)	-	18	-	0.020	-	-
Succinic ~~Acid~~ acid (EESI-)	30 ± 4.0	22	0.68	0.98	1.6 ± 0.10	0.52
Succinic ~~Acid~~ acid (EESI+)	-	26	-	0.029	-	-
Phthalic ~~Acid~~ acid (EESI-)	18~~.1~~ ± 2.8	18	0.41	0.82	0.79 ± 0.070	1.0
Phthalic ~~Acid~~ acid (EESI+)	-	620	-	0.68	-	-
4-nitrophenol (EESI-)*	1.6 ± 0.57	26	0.036	1.2	0.59 ± 0.050	5.9
3-methyl-4-nitrophenol (EESI-)*	5.8 ± 4.0	42	0.14	1.9	0.90 ± 0.10	8.0
Levoglucosan (EESI+)	200 ± 10	900	1.0	1.0	0.45 ± 0.06	-

* The reported values here are highly uncertain due to differences in evaporation for each instrument

Phthalic acid elutes as two isomers, with the largest eluting between 4 and 6 min~~utes~~. All three instruments match well. 4-nitrocatechol was next, and showed very good agreement between the EESI and AMS, but a factor of ~ 2 difference between the SMPS and ~~AMS~~EESI / ~~EESI~~AMS. The exact cause for this discrepancy is unknown.

4-nitrophenol and 3-methyl-4-nitrophenol both match well between the EESI / AMS, but the SMPS concentration is a factor of 20 less than the other two instruments. The likely explanation is that 4-nitrophenol and 3-methyl-4-nitrophenol are volatile (table S2). Compared to succinic acid, > 90 % of these species evaporated from injection to detection by the EESI / AMS. The SMPS measurement is slower than the other instruments, and dilutes

Formatted Table

Formatted: Superscript

Formatted: Superscript

the incoming aerosol by a factor of 4 inside the DMA column. The AMS and EESI measurements are faster and do not dilute the incoming aerosol. Due to these differences, nearly all of the injected mass evaporated in the SMPS. This suggests that volatile species (where C^* >> OA) are not able to be calibrated for by this method. Evaporation would also likely occur during direct calibrations, but to a lesser degree due to the higher pure- species OA concentrations.

Formatted: Superscript

3.2.2 Combined application of the multi-instrumental calibration method and PMF on two mixed standards solutions

PMF was combined with the multi-instrument calibration method to better separate the AMS data for succinic acid and phthalic acid, which overlap in Fig. 4. The results of applying PMF to the AMS data is shown below in Fig. 5. ~~A 6-factor solution was chosen (Fig. 5g).~~

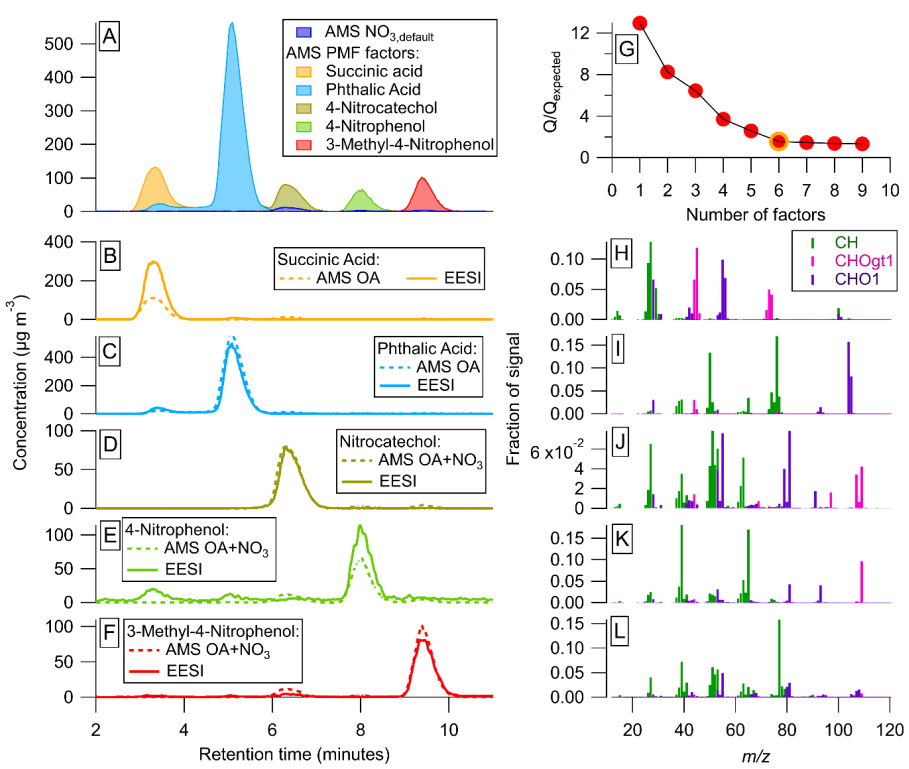

480

Commented [P5]: Delete image, reformatted

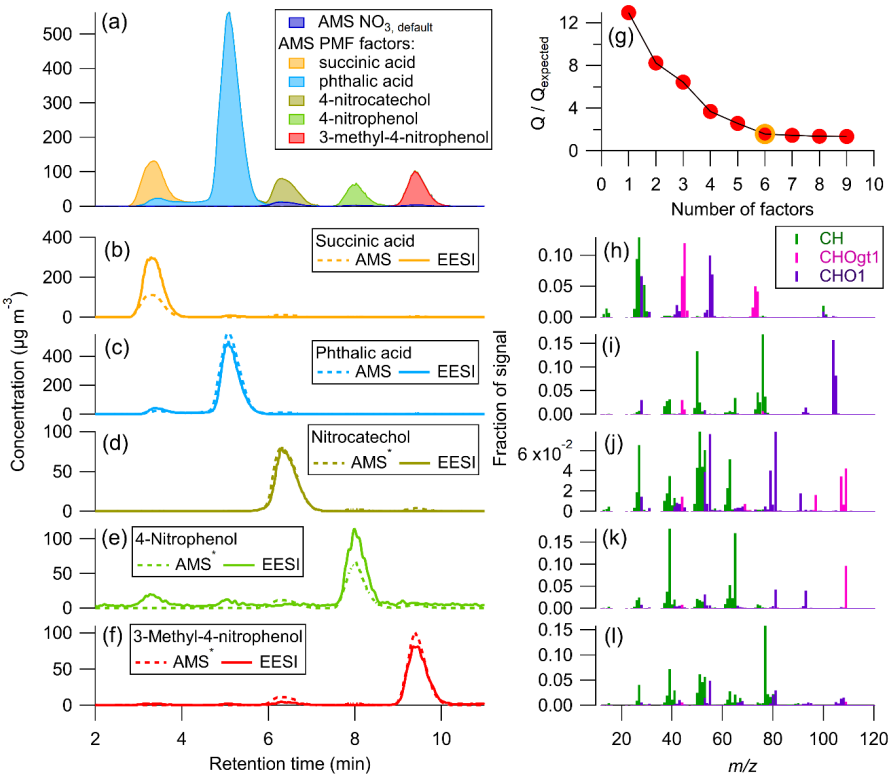

Figure 5. Time series for the AMS PMF solution, (~~A~~a) stacked plot of each factor and AMS NO_3, (~~B~~b) - (~~F~~f) PMF factor with CF_x^A applied to individual species, along with EESI concentrations. (~~G~~g) Q / $Q_{expected}$ vs. number of PMF factors, chosen solution circled in yellow. (~~H~~h) - (~~L~~l) mass spectra (colored by associated AMS HR family) for each AMS PMF factor. A 6 factor solution was chosen, with only 5 factors plotted here. The remaining factor was attributed to the background signal, and was < 2 µg m^{-3} at all times.

*** AMS signal shown is OA + $NO_{3, default}$**

Formatted: Font: (Default) Times New Roman, 9 pt, Bold, Subscript

Figure 5a – Fig. 5f show excellent separation by PMF between the time series for each of the standards present in the mixture. This is likely due to the very different mass spectra for each species (Fig. 5h - Fig. 5l) as well as the time separation achieved by the HPLC. The mass spectra for each standard was compared to the direct calibration mass spectra to confirm the AMS PMF factors were assigned correctly (Fig. S6 and table S4). For all species, there was excellent correspondence, and the uncentered correlation coefficient (UC) between the mass spectral peaks was > 0.95.

Here, the CF_x^A and CF_x^E values are known for each pure standard (from direct calibrations). When applying the *CF* to individual species, the overall agreement between the AMS and EESI time series is comparable to that

shown in Fig. 4. The AMS still underestimates succinic acid by a factor of ~ 2 compared to the EESI, even after better separation is achieved with PMF. As discussed previously, this could be due to the mixing of the two species, which might change the viscosity or phase of the sampled aerosols compared to the pure species, which in turn could fundamentally change the CF_x^A due to the change in CE. Whilst separation was achieved with PMF, PMF time series are likely more accurate for systems where different species have similar CF_x^A (e.g. SOA mixtures from a single precursor and oxidant).

The AMS chromatogram for the mixture studied in Fig. 4 and Fig. 5 was mostly well- separated without PMF. In order to assess the ability of PMF to separate AMS data for a more complex mixture, PMF was run on a different standard solution shown in Fig. 6.

506

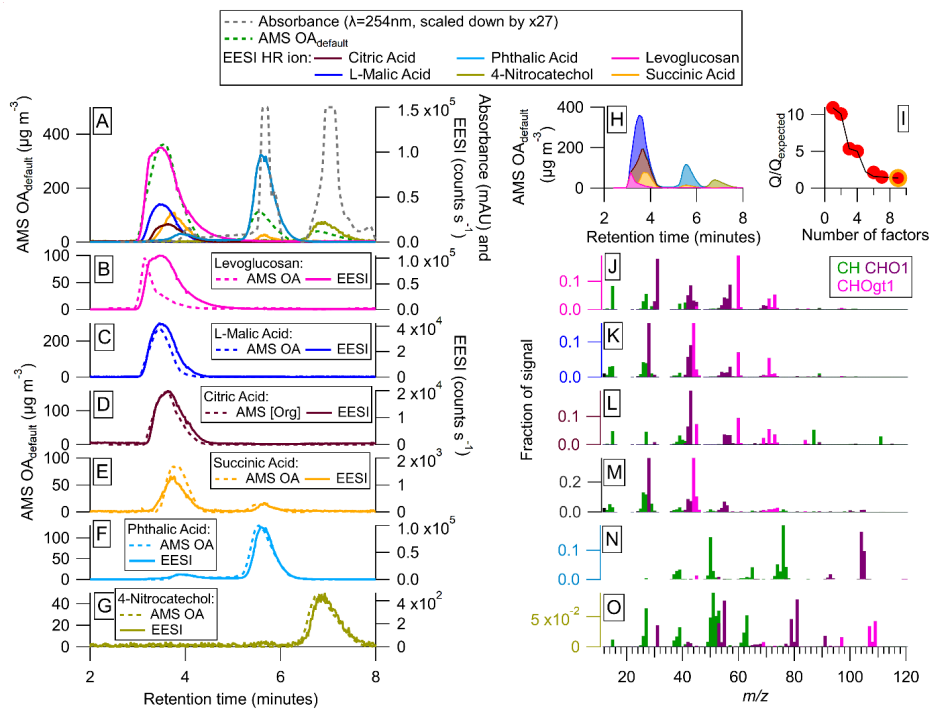

507

Commented [P6]: Deleted image, reformatted

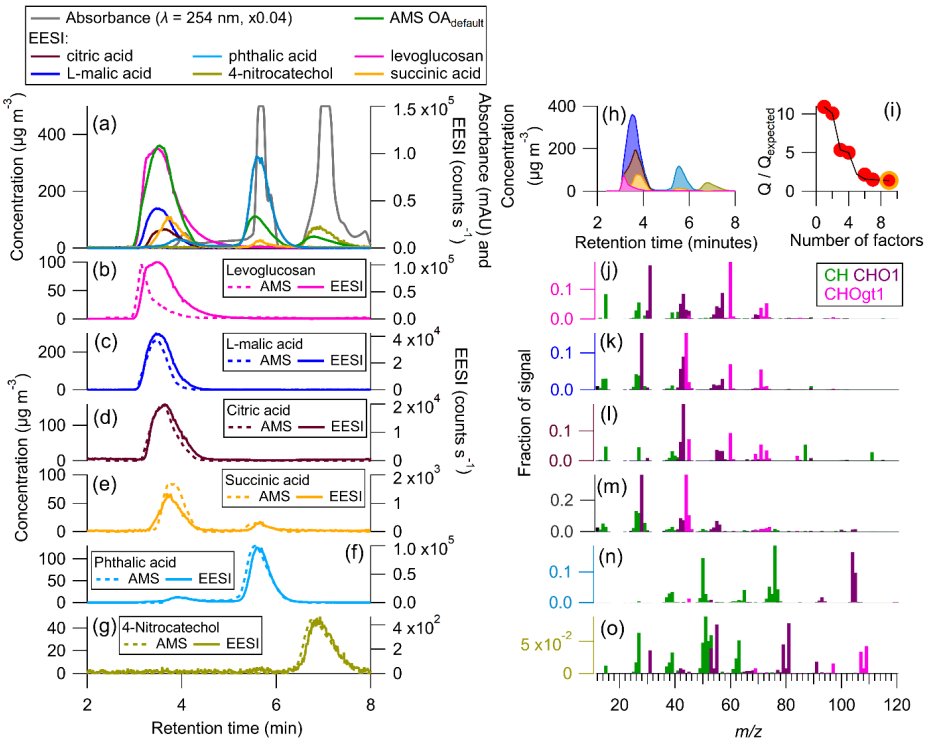

Figure 6. (~~A~~a) time series of AMS total OA (assumed CF_x^A = 1.4), EESI HR ion, and absorbance (max = 4 ×~~×~~ 10^6, milli-absorbance units). (~~B~~b) - (~~G~~g) AMS PMF factor (assumed $CF_x^{A,default}$=1.4) and EESI HR ion for 6 calibrants. (~~H~~h) Stacked PMF factor solution time- series, (~~G~~g) Q / $Q_{exp~~ected~~}$ for AMS PMF solution, a 9 -factor solution was chosen (yellow circle) with FPEAK = 0.2, and (~~J~~j) - (~~O~~o) AMS family- colored mass spectra for 6 PMF factors. For levoglucosan and succinic acid, 2 factors were combined. The remaining factor was attributed to the background signal (< 2 μg m^{-3} at all times).

Formatted: Font: (Default) Times New Roman, 9 pt, Bold

Unlike the data shown in Fig. 3 -– Fig. 5, the species run in the standard solution shown in Fig. 6 were not calibrated directly. Thus, Fig. 6 serves as a test of PMFs ability to resolve AMS data for complex mixtures, rather than a comparison of the calibration methods. Figure 6a shows the uncalibrated time series / chromatogram for the standards in the mixture. In contrast to the previous mixture, this solution contains ~~5~~ five co-eluting peaks: levoglucosan, L-malic acid, citric acid, succinic acid, and a small fraction of the phthalic acid and its isomer. These ~~5~~ five co-eluting peaks suggest that the application of only HPLC with the separation method being used here is not sufficient for these species, likely due to how polar they are. Further separation could be achieved by either changing the HPLC method (through the use of a normal phase chromatography, which uses e.g. a silica column) or running PMF on the AMS data.

Figures 6b – Fig. 6h shows AMS PMF time series for the standards present in the mixture. In Fig. 6b, both the AMS and EESI levoglucosan peaks have different shapes. The EESI peak has a right tail, which is potentially due to the "sticky" (semi-volatile) nature of levoglucosan (Brown et al., 2021). The AMS peak has a sharp increase and slow descent, and does not resemble a Gaussian (which is the approximate shape we expect eluting peaks to have). This is likely due to an imperfect PMF separation. Despite that, when comparing the mass spectra in Fig. 6j to the direct calibration mass spectra in Fig. S7, UC (table S5) is 0.93, suggesting consistency between the two mass spectra.

L-malic acid and citric acid also co-elute with levoglucosan. For citric acid, L-malic acid, and levoglucosanThe PMF factors assigned to those species do look like Gaussian curves, but the mass spectra shown in Fig. 6j – Fig. 6l are somewhat similar. For L-malic acid and levoglucosan, *m/z* 60 makes up some of the observed signal. While *m/z* 60 is a known levoglucosan AMS ion, the direct calibration mass spectra for L-malic acid also shows some signal at *m/z* 60. The PMF mass spectra for L-malic acid has a slightly higher ratio of *m/z* 60 relative to the other ions, which could suggest that there is some mixing between the L-malic acid and levoglucosan factors. The assigned L-malic acid factor has a UC of 0.89 with the directly calibrated mass spectra, but citric acid was not directly calibrated for, and it is likely there is some overlap in the AMS factors between those three species. This was an especially complex solution for PMF to resolve due to the very similar retention times and mass spectra between these species.

As in Fig. 5, succinic acid, phthalic acid, and 4-nitrocatechol (Fig. 6e – Fig. 6g and Fig. 6m – Fig. 6o) are easily resolved when running PMF on the AMS HPLC chromatograms. This is likely due to both the retention time differences and the different AMS mass spectra for these three species. In Table 1, calibration factors are shown for levoglucosan, succinic acid, phthalic acid, and 4-nitrocatechol. CF_x^A is known from the direct calibrations done in Fig. 4. During this experiment, oOnly levoglucosan was cross-calibrated with a direct calibration, however,but the multi-instrumental calibration value is highly affected by the shape of the AMS PMF factor associated with levoglucosan. Thus, the multi-instrumental calibration factor for levoglucosan is likely incorrect. The PMF factor stacked time series is shown in Fig. 6h. These results suggest that while PMF run on the AMS data does provide further peak resolution compared to HPLC alone, PMF cannot completely resolve all co-eluting peaks.

3.3 Combined application of the multi-instrumental calibration method and PMF on β-pinene +/+ NO_3 SOA

In order to test the applicability of the proposed method to a complex real system, SOA from β-pinene + NO_3 was generated, collected on a filter, extracted, and analyzed with our multi-instrument system (per Sect. 2.1). This SOA system has been studied in depth previously and 95 % of the SOA mass is composed of eight unique products, shown in Table 1 in Claflin and Ziemann (2018) and Table S6 here (Claflin and Ziemann, 2018). Of the eight known products, we identified molecular ions that are attributed to a monomer (*m/z* 268.1, assumed to be $[C_{10}H_{15}NO_6\text{-}Na]^+$) and five dimers. Some of the dimers elute as different isomers, but the EESI HR ions observed corresponded to *m/z* 451.2 ($[C_{20}H_{32}N_2O_8\text{-}Na]^+$), *m/z* 467.2 ($[C_{20}H_{32}N_2O_9\text{-}Na]^+$), *m/z* 483.2 ($[C_{20}H_{32}N_2O_{10}\text{-}Na]^+$), and m/z 499.2 ($[C_{21}H_{36}N_2O_{10}\text{-}Na]^+$), all of which were identified in Claflin and Ziemann (2018). We also observed two additional ions, *m/z* 388.2 and *m/z* 465.2, whose structures remain unknown. To better compare the differences in

Formatted: Font: Italic
Formatted: Font: Italic
Formatted: Font: Italic
Formatted: Font: Italic
Formatted: Font: Italic
Formatted: Subscript
Formatted: Subscript
Formatted: Subscript
Formatted: Superscript
Formatted: Font: Italic
Formatted: Subscript
Formatted: Subscript
Formatted: Subscript
Formatted: Subscript
Formatted: Superscript
Formatted: Font: Italic
Formatted: Subscript
Formatted: Subscript
Formatted: Subscript
Formatted: Subscript
Formatted: Superscript
Formatted: Font: Italic
Formatted: Subscript
Formatted: Subscript
Formatted: Subscript
Formatted: Subscript
Formatted: Superscript
Formatted: Subscript
Formatted: Subscript
Formatted: Subscript
Formatted: Subscript
Formatted: Superscript
Formatted: Font: Italic
Formatted: Font: Italic

the chromatogram obtained here vs that shown in Claflin and Ziemann (2018), we compare the UV-Vis time series in Fig. S9. The chromatograms are similar, although their chromatogram had slightly better resolution. Differences in observed species could potentially arise due to the age of the SOA extract used here (~ 1 year) vs. the fresh SOA extract used in that study, fragmentation of species in the EESI (e.g. *m/z* 388.2), or other experimental factors. ~~many of the products have been identified (Claflin and Ziemann, 2018; DeVault et al., 2022). The HPLC method was that of DeVault et al. (2022). Species here are identified based on comparison to the results in the aforementioned papers, and the observed EESI+ HR ions that show peaks in the time series (Fig. 7). Per Claflin and Ziemann (2018), many of the known products are oligomers, formed primarily from the reactions of two carbonyl nitrate monomers.~~ For simplicity, the SOA peaks observed will be referenced by their associated EESI HR io~~n~~.

Formatted: Font: Italic

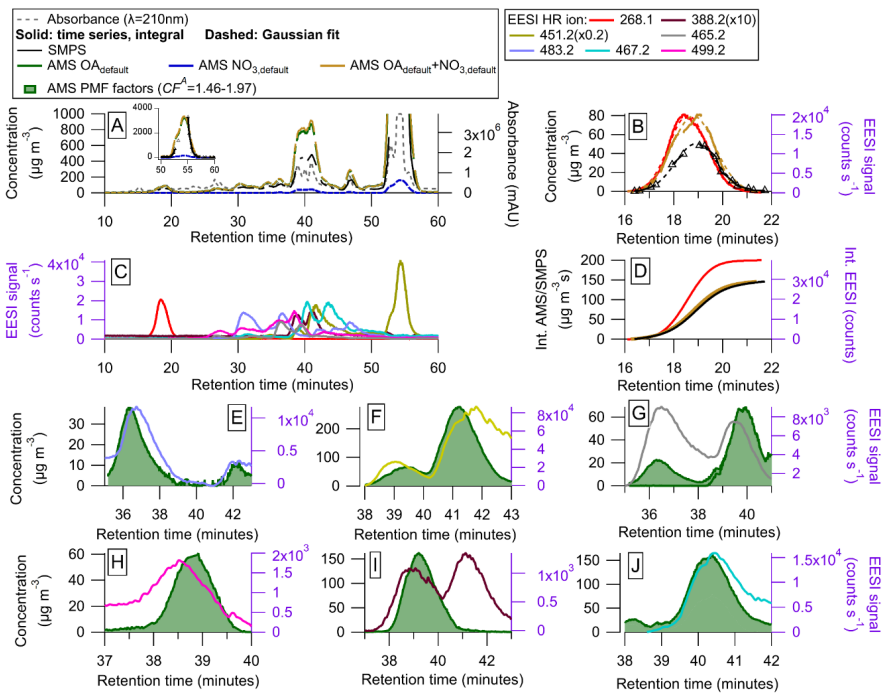

570

Commented [P7]: Deleted image

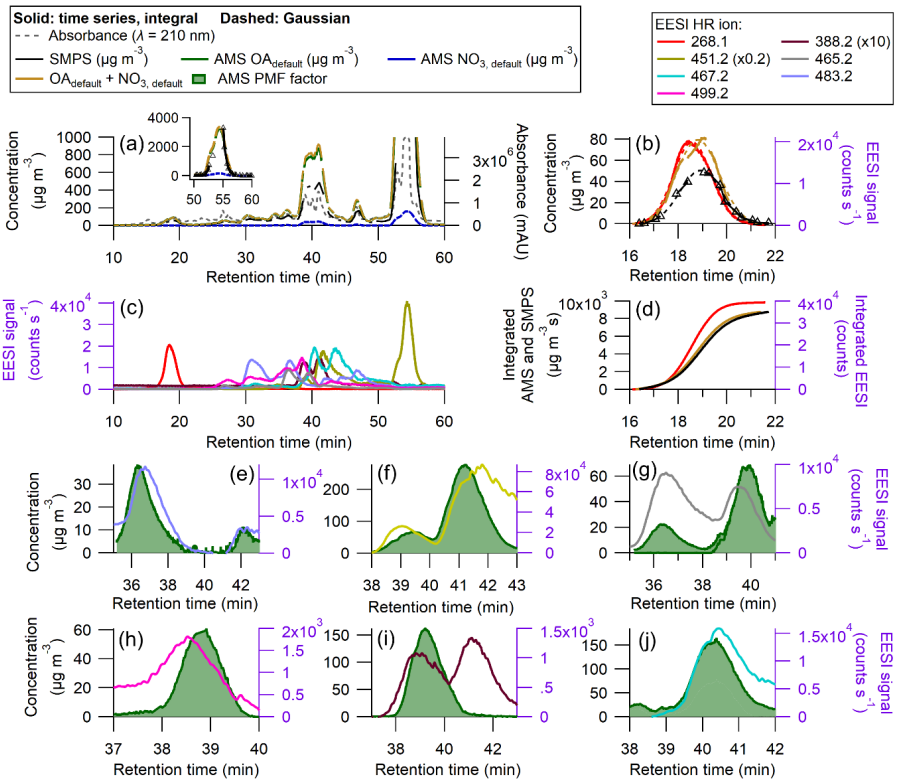

Figure 7. Results of an HPLC run for SOA from β-pinene + NO_3 (~~A~~a) AMS, SMPS, and UV-Vis chromatograms (milli-absorbance units), with inset showing peak from 50 - 60 min~~utes~~. (~~B~~b) Time series and Gaussian fits for the peak between 16 and 20 min~~utes~~ (without using PMF), (~~C~~c) EESI HR ions time series (~~D~~d) time integrated mass concentrations (ion signal) for AMS OA and NO_3, SMPS total mass, and EESI+ HR ion (m/z = 268.1). (~~E~~e) - (~~J~~j) show some AMS PMF factors against measured EESI+ HR ions. (~~G~~g), (~~H~~h), and (~~J~~j) represent split AMS PMF factors for the measured EESI+ HR ions. The AMS PMF factors have a CF_x^A ranging from 1.46 - 1.97 as shown in Fig. S3 and Table 2. Densities are applied to the SMPS data, shown in Fig. S8.

Figure 7a shows the full time- series for the β-pinene system. ~~Many chromatographic peaks are observed by the AMS, SMPS, EESI, and UV-Vis.~~ Many of the peaks are ~~present in clusters and~~ not ~~well enough~~ resolved enough to ~~fit individual~~allow for the direct calculation of CF_x^A and CF_x^E using the SMPS as a the reference, as discussed in Sect. 2.7. ~~Gaussian curves to the EESI and AMS data. Claflin and Ziemann (2018) measured a similar (albeit slightly better separated) UV-Vis chromatogram (Fig. S9). Differences could potentially arise due to the age of the SOA extract used here (~ 1 year) vs. the fresh SOA extract used in that study, or other experimental factors.~~

Formatted: Font: 10 pt

Formatted: Font: 10 pt

Formatted: Font: 10 pt

The degree of peak co-elution is shown~~Overlapping peaks are also observed in the EESI data (~~ in Fig. 7c~~)~~. There are two isolated peaks, ~~from~~ *m/z* 268.1 from 15 - 21 min~~utes~~ and *m/z* 451.2 from 52 - 58 min~~utes~~. ~~One peak, measured at EESI HR ion *m/z* 483.2 (suspected structure shown in table S6), was mostly resolved, and also shows up from ~ 46-48 minutes.~~ The raw (and fitted) data is shown in Fig. 7b for the EESI ion measured at *m/z* 268.1. ~~(a monomer, tricarbonyl nitrate) (Claflin and Ziemann, 2018).~~ The integrated fits are shown in Fig. 7d.

The EESI sensitivities for the overlapping peaks ~~Multiple peaks overlap~~ from ~ 30 to ~ 50 min~~utes (based on the EESI data shown in Fig. 7c).~~ were calculated by referencing the observed EESI signal to the AMS PMF time series. ~~These peaks are likely all dimers, the species identified by Claflin and Ziemann (2018) and measured by the EESI are shown in Table 5. Not every peak observed in Claflin and Ziemann (2018) was identified here, which is likely due to lack of EESI sensitivity to some species and potential decomposition of SOA products (specifically for the trimer identified in Claflin and Ziemann (2018)). In contrast, some EESI HR ions that do not correspond to peaks identified in Claflin and Ziemann (2018) were detected here, but structures for those species are unknown.~~

~~———~~In Fig. 7e – Fig. 7j, AMS PMF time series that increased during~~for~~ the middle third of the run are shown alongside EESI HR ions. The full PMF solution can be found in Fig. S10 – Fig. S12. AMS factors were matched with EESI HR ions based on the retention time and general shape of the time series. For some peaks, the retention times differ by up to 0.5 min. ~~These peaks are assigned based on the similarity in time series between the EESI and AMS.~~ The complexity of this solution, as well as the similarities in the products' molecular structures, likely hindered the ability of PMF to fully resolve each individual product. For many of the overlapping peaks, ~~that overlap the most in time,~~ the magnitude of the individual AMS PMF factors ~~separated during this time a~~are comparable ~~to each other~~.

CF_x^E and CF_x^A are given for each identified species in Table 2. Many of the identified species have CF_x^E in the same range as levoglucosan, within a factor of 3.

Table 2. EESI HR ion, CF_x^E (counts s^{-1} µg^{-1} m^3), CF_x^E / CF_{levo}^E, and~~CF_x^A, and associated PMF factor for the β-pinene + NO_3 SOA mixture.~~. ~~CF_x^A CF_{levo}^E~~. CF_{levo}^E = 441.6 counts s^{-1} µg^{-1} m^3. CF_x^E was calculated using the AMS PMF [~~Org~~OA] ×~~×~~ 1.05 (the average [NO_3] contribution was ~ 5 %, Fig. S3).

~~EESI ion~~	~~CF_x^E (counts s^{-1} µg^{-1} m^3)~~	~~CF_x^E/CF_{levo}^E (unitless)~~	~~CF_x^A (unitless)~~	~~AMS PMF factor(s)~~
~~268.1~~	~~270~~	~~0.61~~	~~1.46~~	~~-~~
~~388.2~~	~~10.9~~	~~0.023~~	~~1.97~~	~~9, 13~~
~~451.2 (1)~~	~~407~~	~~0.92~~	~~1.97~~	~~13~~
~~451.2 (2)~~	~~423~~	~~0.96~~	~~1.73~~	~~13~~
~~451.2 (3)~~	~~83.2~~	~~0.19~~	~~1.97*~~	~~-~~
~~465.2 (1)~~	~~670~~	~~1.5~~	~~1.97~~	~~2~~
~~465.2 (2)~~	~~170~~	~~0.38~~	~~1.97~~	~~10~~

Formatted: Indent: First line: 0"

~~467.2~~	~~139~~	~~0.31~~	~~1.73~~	~~5,8~~
~~483.2~~	~~435~~	~~0.99~~	~~1.97~~	~~14~~
~~499.2~~	~~54.2~~	~~0.12~~	~~1.97~~	~~12~~

~~* Incomplete SMPS data, assuming CF_x^A=1.97.~~

EESI ion	CF_x^E (counts s^{-1} μg^{-1} m^3)	CF_x^E / CF_{levo}^E (unitless)	CF_x^A (unitless)
268.1	270	0.61	1.46
388.2	10.9	0.023	1.97
451.2 (1)	407	0.92	1.97
451.2 (2)	423	0.96	1.73
451.2 (3)	83.2	0.19	1.97*
465.2 (1)	670	1.5	1.97
465.2 (2)	170	0.38	1.97
467.2	139	0.31	1.73
483.2	435	0.99	1.97
499.2	54.2	0.12	1.97

* Incomplete SMPS data, assuming CF_x^A=1.97.

Formatted Table

Formatted: Font: 9 pt, Not Italic

Some species, like the EESI HR ions measured at *m/z* 388.2 and *m/z* 499.2, have much lower EESI sensitivity than the other species. These species could be fragments of a larger parent ion, or they could be species that, for whatever reason, do not form a strong adduct with Na^+. The ambiguity in the PMF factors may result in some errors in CF_x^E, but they are unlikely to fully explain the factor of 10~~ten~~ difference in sensitivity between the most and least sensitive β-pinene + NO_3 products. In future runs with slightly better chromatographic separation a multi-variate fit of individual factors vs. the SMPS may allow further constraining the quantification.

In this system, many of the products differ only by one or two oxygen atoms. ~~Some may contain a~~ In some cases, a carboxylic acid functional group replaces~~in the place of~~ a ketone, whilst ~~others~~ other molecules contain a cyclic ether, and some do not. The subtle differences in structure could influence the sensitivity with the EESI, as the oxygenated moieties may change the likelihood of forming a strong $[M+Na]^+$ adduct. Further, some EESI HR ions eluted multiple times (e.g. *m/z* 451.2). Claflin and Ziemann (2018) identified the structure of this ion for the third peak (shown in Table S6). However, this ion is measured twice more, from 38 - 43 min~~utes~~, which suggests the presence of isomers. Isomers can have different structures (shown in Table S6) and different CF_x^E. One example is *m/z* 483.2, where one isomer has a CF_x^E = 327.2 and a second isomer has a CF_x^E = 54.2 counts s^{-1} μg^{-1} m^3. ~~Due to the chromatographic separation between these peaks and the third peak, it is likely that the first two species are some~~

Formatted: Font: Italic

Formatted: Superscript

Formatted: Superscript

Formatted: Superscript

~~isomeric form of the species identified in Claflin and Ziemann (2018). As is shown for *m/z* 483.2 (Table S6), isomers can have different structures and very different CF_x^E (327.2 vs. 54.2 counts s^{-1} μg^{-1} m^3).~~

Despite differences in CF_x^E, CF_x^A was more consistent. In table 2, the AMS response to different SOA species formed from a single VOC precursor varies only by 25 %. For the mixed peaks ~~(individual EESI *m/z*'s shown in Fig. 7e-7j),~~ CF_x^A was either 1.~~48~~ 97 or 1.~~58~~73, as ~~shown~~ discussed in Sect. S3 and~~in~~ shown in Fig. S3. ~~For the three isolated peaks (*m/z* 268.2, *m/z* 451.2 [peak 3], and *m/z* 483.2 [peak 2]), the CF_x^A spanned from 1.31 to 1.75.~~ For one of the isolated peaks, *m/z* 451.2, ~~(peak 3),~~ the actual CF_x^A was not calculated, due to a malfunction of the SMPS system between 54 - 56 min~~utes~~. Individual peaks' Gaussian fits and integrated curves are shown in Fig. S13.

3.4 Discussion on the application of this method

In this paper, a novel technique was introduced that allows for the calibration of real-time mass spectrometers for individual species that cannot be obtained directly. This paper addresses the feasibility, performance, and limitations of this technique, all of which are necessary for any future use of this method.

The original purpose of this method was to calibrate species in SOA formed from laboratory chamber experiments. In many cases, the identity of the species was unknown, or the species could not be purchased as a pure standard. During those chamber experiments, SOA composition was measured in real-time with AMS, EESI, and SMPSs. SOA was also pulled through a Teflon filter, extracted in solvent, injected into the HPLC.

One application of this method would allow calculating yields for different SOA species produced from the oxidation of individual VOCs. This would allow for a better understanding of the chemical and partitioning mechanisms controlling the SOA composition and formation, along with providing information on which species are contributing the most to environmental and human health issues caused by SOA (e.g. higher light absorption or increased toxicity).

Another application is inferring calibration factors for important species in field datasets. This could be done by collecting filters to use with this method, including using UPLC for higher resolution. Alternatively, if specific primary sources or SOA precursors are known to be important for a dataset, those can be sampled in the lab to determine key species and their calibration factors.

One example of a field application is the FIREX-AQ field campaign, where the Jimenez lab at the Univ. of Colorado Boulder operated an EESI (Pagonis et al., 2021). During that campaign, direct calibrations were performed daily using either 4-nitrocatechol or levoglucosan. In the laboratory, these calibrations were also carried out daily, before chamber experiments and before running the HPLC calibration method. If species specific sensitivities are obtained in the lab, then they can be ratioed to either 4-nitrocatechol or levoglucosan, providing the relative sensitivity of individual analytes. The relative sensitivity can be referenced to the sensitivities obtained in the field, allowing for the budgeting of ambient SOA for multiple species.

4 Conclusions

Formatted: Space Before: 12 pt, After: 12 pt

Formatted: Font: Not Bold

Formatted: Indent: First line: 0.5"

Formatted: Font: Not Bold

Formatted: Font: Not Bold

Formatted: Font: Not Bold

Formatted: Font: Not Bold

Formatted: Font: Not Bold

~~A~~ In this study, we introduced a novel multi-instrumental calibration method for EESI and AMS~~has been demonstrated here,~~ that uses ~~the~~ HPLC and PMF to separate complex standard mixtures and SOA into individual species or sub groups of species present in the mixture. ~~chemical separation power of the HPLC, combined with analytical aerosol detection of SMPS, AMS, and EESI to calibrate the mass spectrometers for individual species in mixtures. When running~~ Our proof of concept test using individual pure standards demonstrated close agreement (within 20 %) between direct and multi-instrumental calibration factors, indicating this method's quantitative ability. In a second proof of concept using a mostly resolved standard mixture, EESI direct and multi-instrumental calibration factors agree within a factor of two for low volatility species. We note that this method is not suitable for semivolatile species whose C^* is similar or higher than the concentration of aerosol sampled inside the SMPS DMA column. These results suggest that this method can be used to reliably determine species sensitivities for completely and mostly resolved chromatograms.~~individual standards, the multi-instrumental calibration method agreed with direct calibration within 20%. As the sensitivities of EESI measured species can vary by over an order of magnitude, quantification within 20% is very useful. In a mixed standard run that contained mostly resolved species, the EESI and SMPS agreed within a factor of 1.5 (for non-volatile species). The AMS and EESI matched moderately well, except when measuring succinic acid.~~

When HPLC alone failed to fully resolve individual analytes, ~~In situations where the HPLC column/method was unable to fully separate injected components,~~ PMF on AMS data successfully resolved individual analytes time series in a simple standard mixture. However, in more complex standard and SOA mixtures, while PMF provided some additional chromatographic separation, the PMF solution showed signs of factor mixing. This was especially evident in the ~~was used to methodically compare the time series and mass spectra for different species, and generate time resolved OA data for the AMS. This was especially important for the AMS data, as overlapping peaks are measured as large and wide "total OA" peaks for that instrument.~~

~~The~~ β-pinene ~~+ NO_3~~ SOA ~~solution~~mixture, which contained many similar analytes, ~~was the most complex mixture studied here,~~resulting in a less well resolved PMF solution. ~~primarily due to the suspected presence of many isomers. The majority of the SOA peaks overlapped during the middle third of the HPLC run. PMF separation~~ While approximate EESI and AMS calibration factors were obtained, these sensitivities are affected by the inherent error in the PMF solution. ~~conducted on the HPLC-separate AMS results produced a more complicated solution than the AMS PMF done on the standards' runs. This was likely due to similarities in mass spectra and retention times for the overlapping peaks. Despite that analytical challenge, when the middle third of the chromatogram was scrutinized using both the AMS PMF solution and the measured EESI+ HR ions, approximate calibration factors were obtained.~~In practice, while some mixtures may be adequately resolved by HPLC alone, AMS PMF can improve the chemical resolution of complex systems.

Future studies should prioritize improving the chromatography for the system of interest, potentially through changing the column type and / or mobile phase gradients, or using systems with higher intrinsic resolution such as UPLC (Kenseth et al., 2023). ~~For future studies, additional effort should be focused on tuning the HPLC performance (e.g. through changing the column or mobile phase gradients) that provides higher resolution for whatever system is being studied. In this demonstration project~~ During the experiments shown in this manuscript we

Formatted: Indent: First line: 0"

were limited to a C_{18} column, ~~which is most often used~~which is primarily suited for separating less polar species. ~~In many situations, especially when there is~~However, in the polar standard mixtures shown here and in scenarios involving significant oxidation and smaller precursor gases, the resulting products are likely to~~o be more~~ polar to be adequately~~than can be~~ separated by a C_{18} column. In those experiments, a column with a polar stationary phase would allow for the separation of SOA components. ~~In future experiments, columns with more polar stationary phases should be considered. If HPLC separation alone could completely resolve all chemical peaks, then PMF would not be needed, however in practice it is likely to help the chemical resolution of complex systems.~~

In conclusion, our method offers a valuable tool for quantifying EESI and AMS sensitivities in mixtures, especially pertinent for laboratory generated SOA lacking pure standards or characterized by unknown isomeric forms. This technique can also be applied to other real-time aerosol mass spectrometers. To our knowledge, this technique stands as one of very few available methods for rapid calibration of EESI and AMS for SOA species that are unavailable as pure standards, emphasizing its significance in atmospheric research.~~These results introduce a new technique for better quantifying the instrument responses of the EESI and AMS to different molecular species present in complex mixtures such as from biomass burning, urban, and/or biogenic SOA.~~

Formatted: Font: (Default) Times New Roman, Font color: Auto

Formatted: Font color: Auto

Formatted: Font: (Default) Times New Roman, Font color: Auto

5 Acknowledgements

We thank Harald Stark for data analysis support for Igor and Tofware. This work was supported by NASA grants 80NSSC18K0630, 80NSSC23K0828, and 80NSSC21K1451, a NASA Future Investigators in Earth and Space Science and Technology graduate student research grant (FINESST, 80NSSC20K1642), NSF AGS-2206655, and a CIRES graduate research fellowship.

6 Author Contributions

MKS, DAD, JLJ, and PJZ designed the experiments, MKS carried them out with support from DAD, DK, SY, and PCJ. ACZ, PJZ, and MPD provided the HPLC instrument support. MKS carried out all data analysis and preparation of the manuscript, with contributions from all coauthors.

7 Competing Interests

The authors declare that they have no conflict of interest.

References

Bakker-Arkema, J. G. and Ziemann, P. J.: Minimizing Errors in Measured Yields of Particle-Phase Products Formed in Environmental Chamber Reactions: Revisiting the Yields of β-Hydroxynitrates Formed from 1-Alkene + OH/NOx Reactions, ACS Earth Space Chem., 5(3), 690–702, doi:10.1021/acsearthspacechem.1c00008, 2021.

Brown, W. L., Day, D. A., Stark, H., Pagonis, D., Krechmer, J. E., Liu, X., Price, D. J., Katz, E. F., DeCarlo, P. F., Masoud, C. G., Wang, D. S., Hildebrandt Ruiz, L., Arata, C., Lunderberg, D. M., Goldstein, A. H., Farmer, D. K., Vance, M. E. and Jimenez, J. L.: Real-time organic aerosol chemical speciation in the indoor environment using extractive electrospray ionization mass spectrometry, Indoor Air, 31(1), 141–155, doi:10.1111/ina.12721, 2021.

Canagaratna, M. R., Jayne, J. T., Jimenez, J. L., Allan, J. D., Alfarra, M. R., Zhang, Q., Onasch, T. B., Drewnick, F., Coe, H., Middlebrook, A., Delia, A., Williams, L. R., Trimborn, A. M., Northway, M. J., DeCarlo, P. F., Kolb, C. E., Davidovits, P. and Worsnop, D. R.: Chemical and microphysical characterization of ambient aerosols with the aerodyne aerosol mass spectrometer, Mass Spectrom. Rev., 26(2), 185–222, doi:10.1002/mas.20115, 2007.

Canagaratna, M. R., Jimenez, J. L., Kroll, J. H., Chen, Q., Kessler, S. H., Massoli, P., Hildebrandt Ruiz, L., Fortner, E., Williams, L. R., Wilson, K. R., Surratt, J. D., Donahue, N. M., Jayne, J. T. and Worsnop, D. R.: Elemental ratio measurements of organic compounds using aerosol mass spectrometry: characterization, improved calibration, and implications, Atmos. Chem. Phys., 15(1), 253–272, doi:10.5194/acp-15-253-2015, 2015.

Chen, H., Venter, A. and Graham Cooks, R.: Extractive electrospray ionization for direct analysis of undiluted urine, milk and other complex mixtures without sample preparation, Chem. Commun. , (19), 2042–2044, doi:10.1039/B602614A, 2006.

Claflin, M. S. and Ziemann, P. J.: Identification and Quantitation of Aerosol Products of the Reaction of β-Pinene with NO3 Radicals and Implications for Gas- and Particle-Phase Reaction Mechanisms, J. Phys. Chem. A, 122(14), 3640–3652, doi:10.1021/acs.jpca.8b00692, 2018.

Craven, J. S., Yee, L. D., Ng, N. L., Canagaratna, M. R., Loza, C. L., Schilling, K. A., Yatavelli, R. L. N., Thornton, J. A., Ziemann, P. J., Flagan, R. C. and Seinfeld, J. H.: Analysis of secondary organic aerosol formation and aging using positive matrix factorization of high-resolution aerosol mass spectra: application to the dodecane low-NO_x system, Atmos. Chem. Phys., 12(24), 11795–11817, doi:10.5194/acp-12-11795-2012, 2012.

Day, D. A., Fry, J. L., Kang, H. G., Krechmer, J. E., Ayres, B. R., Keehan, N. I., Thompson, S. L., Hu, W., Campuzano-Jost, P., Schroder, J. C., Stark, H., DeVault, M. P., Ziemann, P. J., Zarzana, K. J., Wild, R. J., Dubè, W. P., Brown, S. S. and Jimenez, J. L.: Secondary Organic Aerosol Mass Yields from NO3 Oxidation of α-Pinene and Δ-Carene: Effect of RO2 Radical Fate, J. Phys. Chem. A, 126(40), 7309–7330, doi:10.1021/acs.jpca.2c04419, 2022.

DeCarlo, P. F., Slowik, J. G., Worsnop, D. R., Davidovits, P. and Jimenez, J. L.: Particle Morphology and Density Characterization by Combined Mobility and Aerodynamic Diameter

Formatted: Normal, Space After: 0 pt, Line spacing: 1.5 lines

764 Measurements. Part 1: Theory, Aerosol Sci. Technol., 38(12), 1185–1205,
765 doi:10.1080/027868290903907, 2004.

766 DeCarlo, P. F., Kimmel, J. R., Trimborn, A., Northway, M. J., Jayne, J. T., Aiken, A. C., Gonin,
767 M., Fuhrer, K., Horvath, T., Docherty, K. S., Worsnop, D. R. and Jimenez, J. L.: Field-
768 deployable, high-resolution, time-of-flight aerosol mass spectrometer, Anal. Chem., 78(24),
769 8281–8289, doi:10.1021/ac061249n, 2006.

770 DeVault, M. P., Ziola, A. C. and Ziemann, P. J.: Products and Mechanisms of Secondary
771 Organic Aerosol Formation from the NO3 Radical-Initiated Oxidation of Cyclic and Acyclic
772 Monoterpenes, ACS Earth Space Chem., 6(8), 2076–2092,
773 doi:10.1021/acsearthspacechem.2c00130, 2022.

774 Docherty, K. S., Jaoui, M., Corse, E., Jimenez, J. L., Offenberg, J. H., Lewandowski, M. and
775 Kleindienst, T. E.: Collection Efficiency of the Aerosol Mass Spectrometer for Chamber-
776 Generated Secondary Organic Aerosols, Aerosol Sci. Technol., 47(3), 294–309,
777 doi:10.1080/02786826.2012.752572, 2013.

778 Dockery, D. W., Cunningham, J., Damokosh, A. I., Neas, L. M., Spengler, J. D., Koutrakis, P.,
779 Ware, J. H., Raizenne, M. and Speizer, F. E.: Health effects of acid aerosols on North American
780 children: respiratory symptoms, Environ. Health Perspect., 104(5), 500–505,
781 doi:10.1289/ehp.96104500, 1996.

782 Dzepina, K., Arey, J., Marr, L. C., Worsnop, D. R., Salcedo, D., Zhang, Q., Onasch, T. B.,
783 Molina, L. T., Molina, M. J. and Jimenez, J. L.: Detection of particle-phase polycyclic aromatic
784 hydrocarbons in Mexico City using an aerosol mass spectrometer, Int. J. Mass Spectrom., 263(2–
785 3), 152–170, doi:10.1016/j.ijms.2007.01.010, 2007.

786 Eichler, P., Müller, M., D'Anna, B. and Wisthaler, A.: A novel inlet system for online chemical
787 analysis of semi-volatile submicron particulate matter, Atmos. Meas. Tech., 8(3), 1353–1360,
788 doi:10.5194/amt-8-1353-2015, 2015.

789 Farmer, D. K., Matsunaga, A., Docherty, K. S., Surratt, J. D., Seinfeld, J. H., Ziemann, P. J. and
790 Jimenez, J. L.: Response of an aerosol mass spectrometer to organonitrates and organosulfates
791 and implications for atmospheric chemistry, Proc. Natl. Acad. Sci. U. S. A., 107(15), 6670–6675,
792 doi:10.1073/pnas.0912340107, 2010.

793 Gallimore, P. J. and Kalberer, M.: Characterizing an Extractive Electrospray Ionization (EESI)
794 Source for the Online Mass Spectrometry Analysis of Organic Aerosols, Environ. Sci. Technol.,
795 47(13), 7324–7331, doi:10.1021/es305199h, 2013.

796 Gao, Y., Walker, M. J., Barrett, J. A., Hosseinaei, O., Harper, D. P., Ford, P. C., Williams, B. J.
797 and Foston, M. B.: Analysis of gas chromatography/mass spectrometry data for catalytic lignin
798 depolymerization using positive matrix factorization, Green Chem., 20(18), 4366–4377,
799 doi:10.1039/C8GC01474D, 2018.

800 Guo, H., Campuzano-Jost, P., Nault, B. A., Day, D. A., Schroder, J. C., Kim, D., Dibb, J. E.,
801 Dollner, M., Weinzierl, B. and Jimenez, J. L.: The importance of size ranges in aerosol

instrument intercomparisons: a case study for the Atmospheric Tomography Mission, Atmos. Meas. Tech., 14(5), 3631–3655, doi:10.5194/amt-14-3631-2021, 2021.

IPCC: IPCC 2013: Climate Change 2013: The Physical Science Basis. Contribution of Working Group I to the Fifth Assessment Report of the Intergovernmental Panel on Climate Change, edited by T. F. Stocker, D. Qin, G. K. Plattner, M. Tignor, S. K. Allen, V. Bex, and P. M. Midgley, Cambridge University Press, Cambridge, United Kingdom and New York, NY, USA., 2013.

Jayne, J. T., Leard, D. C., Zhang, X., Davidovits, P., Smith, K. A., Kolb, C. E. and Worsnop, D. R.: Development of an Aerosol Mass Spectrometer for Size and Composition Analysis of Submicron Particles, Aerosol Sci. Technol., 33(1–2), 49–70, doi:10.1080/027868200410840, 2000.

Jimenez, J. L., Canagaratna, M. R., Donahue, N. M., Prevot, A. S. H., Zhang, Q., Kroll, J. H., DeCarlo, P. F., Allan, J. D., Coe, H., Ng, N. L., Aiken, A. C., Docherty, K. S., Ulbrich, I. M., Grieshop, A. P., Robinson, A. L., Duplissy, J., Smith, J. D., Wilson, K. R., Lanz, V. A., Hueglin, C., Sun, Y. L., Tian, J., Laaksonen, A., Raatikainen, T., Rautiainen, J., Vaattovaara, P., Ehn, M., Kulmala, M., Tomlinson, J. M., Collins, D. R., Cubison, M. J., Dunlea, E. J., Huffman, J. A., Onasch, T. B., Alfarra, M. R., Williams, P. I., Bower, K., Kondo, Y., Schneider, J., Drewnick, F., Borrmann, S., Weimer, S., Demerjian, K., Salcedo, D., Cottrell, L., Griffin, R., Takami, A., Miyoshi, T., Hatakeyama, S., Shimono, A., Sun, J. Y., Zhang, Y. M., Dzepina, K., Kimmel, J. R., Sueper, D., Jayne, J. T., Herndon, S. C., Trimborn, A. M., Williams, L. R., Wood, E. C., Middlebrook, A. M., Kolb, C. E., Baltensperger, U. and Worsnop, D. R.: Evolution of organic aerosols in the atmosphere, Science, 326(5959), 1525–1529, doi:10.1126/science.1180353, 2009.

Jimenez, J. L., Canagaratna, M. R., Drewnick, F., Allan, J. D., Alfarra, M. R., Middlebrook, A. M., Slowik, J. G., Zhang, Q., Coe, H., Jayne, J. T. and Worsnop, D. R.: Comment on "The effects of molecular weight and thermal decomposition on the sensitivity of a thermal desorption aerosol mass spectrometer," Aerosol Sci. Technol., 50(9), i–xv, doi:10.1080/02786826.2016.1205728, 2016.

Kanakidou, M., Seinfeld, J. H., Pandis, S. N., Barnes, I., Dentener, F. J., Facchini, M. C., Van Dingenen, R., Ervens, B., Nenes, A., Nielsen, C. J., Swietlicki, E., Putaud, J. P., Balkanski, Y., Fuzzi, S., Horth, J., Moortgat, G. K., Winterhalter, R., Myhre, C. E. L., Tsigaridis, K., Vignati, E., Stephanou, E. G. and Wilson, J.: Organic aerosol and global climate modelling: a review, Atmos. Chem. Phys., 5(4), 1053–1123, doi:10.5194/acp-5-1053-2005, 2005.

Kenseth, C. M., Hafeman, N. J., Rezgui, S. P., Chen, J., Huang, Y., Dalleska, N. F., Kjaergaard, H. G., Stoltz, B. M., Seinfeld, J. H. and Wennberg, P. O.: Particle-phase accretion forms dimer esters in pinene secondary organic aerosol, Science, 382(6672), 787–792, doi:10.1126/science.adi0857, 2023.

Kimmel, J. R., Farmer, D. K., Cubison, M. J., Sueper, D., Tanner, C., Nemitz, E., Worsnop, D. R., Gonin, M. and Jimenez, J. L.: Real-time aerosol mass spectrometry with millisecond resolution, Int. J. Mass Spectrom., 303(1), 15–26, doi:10.1016/j.ijms.2010.12.004, 2011.

Kruve, A., Kaupmees, K., Liigand, J. and Leito, I.: Negative electrospray ionization via deprotonation: predicting the ionization efficiency, Anal. Chem., 86(10), 4822–4830, doi:10.1021/ac404066v, 2014.

Kumar, V., Giannoukos, S., Haslett, S. L., Tong, Y., Singh, A., Bertrand, A., Lee, C. P., Wang, D. S., Bhattu, D., Stefenelli, G., Dave, J. S., Puthussery, J. V., Qi, L., Vats, P., Rai, P., Casotto, R., Satish, R., Mishra, S., Pospisilova, V., Mohr, C., Bell, D. M., Ganguly, D., Verma, V., Rastogi, N., Baltensperger, U., Tripathi, S. N., Prévôt, A. S. H. and Slowik, J. G.: Highly time-resolved chemical speciation and source apportionment of organic aerosol components in Delhi, India, using extractive electrospray ionization mass spectrometry, Atmos. Chem. Phys., 22(11), 7739–7761, doi:10.5194/acp-22-7739-2022, 2022.

Kuwata, M., Zorn, S. R. and Martin, S. T.: Using elemental ratios to predict the density of organic material composed of carbon, hydrogen, and oxygen, Environ. Sci. Technol., 46(2), 787–794, doi:10.1021/es202525q, 2012.

Lanz, V. A., Alfarra, M. R., Baltensperger, U., Buchmann, B., Hueglin, C. and Prévôt, A. S. H.: Source apportionment of submicron organic aerosols at an urban site by factor analytical modelling of aerosol mass spectra, Atmos. Chem. Phys., 7(6), 1503–1522, doi:10.5194/acp-7-1503-2007, 2007.

Law, W. S., Wang, R., Hu, B., Berchtold, C., Meier, L., Chen, H. and Zenobi, R.: On the mechanism of extractive electrospray ionization, Anal. Chem., 82(11), 4494–4500, doi:10.1021/ac100390t, 2010.

Lee, E., Chan, C. K. and Paatero, P.: Application of positive matrix factorization in source apportionment of particulate pollutants in Hong Kong, Atmos. Environ., 33(19), 3201–3212, doi:10.1016/S1352-2310(99)00113-2, 1999.

Lighty, J. S., Veranth, J. M. and Sarofim, A. F.: Combustion aerosols: factors governing their size and composition and implications to human health, J. Air Waste Manag. Assoc., 50(9), 1565–618; discussion 1619-22 [online] Available from: https://www.ncbi.nlm.nih.gov/pubmed/11055157, 2000.

Liigand, J., Wang, T., Kellogg, J., Smedsgaard, J., Cech, N. and Kruve, A.: Quantification for non-targeted LC/MS screening without standard substances, Sci. Rep., 10(1), 5808, doi:10.1038/s41598-020-62573-z, 2020.

Liu, X., Day, D. A., Krechmer, J. E., Brown, W., Peng, Z., Ziemann, P. J. and Jimenez, J. L.: Direct measurements of semi-volatile organic compound dynamics show near-unity mass accommodation coefficients for diverse aerosols, Communications Chemistry, 2(1), 1–9, doi:10.1038/s42004-019-0200-x, 2019.

Lohmann, U., Broekhuizen, K., Leaitch, R., Shantz, N. and Abbatt, J.: How efficient is cloud droplet formation of organic aerosols?, Geophys. Res. Lett., 31(5), 2004.

Lopez-Hilfiker, F. D., Mohr, C., Ehn, M., Rubach, F., Kleist, E., Wildt, J., Mentel, T. F., Lutz, A., Hallquist, M., Worsnop, D. and Thornton, J. A.: A novel method for online analysis of gas

879 and particle composition: description and evaluation of a Filter Inlet for Gases and AEROsols
880 (FIGAERO), Atmos. Meas. Tech., 7(4), 983–1001, doi:10.5194/amt-7-983-2014, 2014.

881 Lopez-Hilfiker, F. D., Pospisilova, V., Huang, W., Kalberer, M., Mohr, C., Stefenelli, G.,
882 Thornton, J. A., Baltensperger, U., Prevot, A. S. H. and Slowik, J. G.: An extractive electrospray
883 ionization time-of-flight mass spectrometer for online measurement of atmospheric particles,
884 Atmos. Meas. Tech., 12(9), 4867–4886, doi:10.5194/amt-12-4867-2019, 2019.

885 Nault, B. A., Campuzano-Jost, P., Day, D. A., Schroder, J. C., Anderson, B., Beyersdorf, A. J.,
886 Blake, D. R., Brune, W. H., Choi, Y., Corr, C. A., Gouw, J. A. de, Dibb, J., DiGangi, J. P.,
887 Diskin, G. S., Fried, A., Huey, L. G., Kim, M. J., Knote, C. J., Lamb, K. D., Lee, T., Park, T.,
888 Pusede, S. E., Scheuer, E., Thornhill, K. L., Woo, J.-H. and Jimenez, J. L.: Secondary organic
889 aerosol production from local emissions dominates the organic aerosol budget over Seoul, South
890 Korea, during KORUS-AQ, Atmos. Chem. Phys., 18(24), 17769–17800, doi:10.5194/acp-18-
891 17769-2018, 2018.

892 Nault, B. A., Croteau, P., Jayne, J., Williams, A., Williams, L., Worsnop, D., Katz, E. F.,
893 DeCarlo, P. F. and Canagaratna, M.: Laboratory evaluation of organic aerosol relative ionization
894 efficiencies in the aerodyne aerosol mass spectrometer and aerosol chemical speciation monitor,
895 Aerosol Sci. Technol., 1–17, doi:10.1080/02786826.2023.2223249, 2023.

896 Paatero, P.: Least squares formulation of robust non-negative factor analysis, Chemometrics
897 Intellig. Lab. Syst., 37(1), 23–35, doi:10.1016/S0169-7439(96)00044-5, 1997.

898 Paatero, P.: The Multilinear Engine: A Table-Driven, Least Squares Program for Solving
899 Multilinear Problems, including the n-Way Parallel Factor Analysis Model, J. Comput. Graph.
900 Stat., 8(4), 854–854, doi:10.2307/1390831, 1999.

901 Paatero, P.: End user's guide to multilinear engine applications, University of Helsinki, Helsinki,
902 Finland., 2007.

903 Paatero, P. and Tapper, U.: Positive Matrix Factorization - A Nonnegative Factor Model With
904 Optimal Utilization of Error-Estimates of Data Values, Environmetrics, 5(2), 111–126, 1994.

905 Pagonis, D., Campuzano-Jost, P., Guo, H., Day, D. A., Schueneman, M. K., Brown, W. L.,
906 Nault, B. A., Stark, H., Siemens, K., Laskin, A., Piel, F., Tomsche, L., Wisthaler, A., Coggon,
907 M. M., Gkatzelis, G. I., Halliday, H. S., Krechmer, J. E., Moore, R. H., Thomson, D. S.,
908 Warneke, C., Wiggins, E. B. and Jimenez, J. L.: Airborne extractive electrospray mass
909 spectrometry measurements of the chemical composition of organic aerosol, Atmospheric
910 Measurement Techniques, 14(2), 1545–1559, doi:10.5194/amt-14-1545-2021, 2021.

911 Pospisilova, V., Lopez-Hilfiker, F. D., Bell, D. M., El Haddad, I., Mohr, C., Huang, W.,
912 Heikkinen, L., Xiao, M., Dommen, J., Prevot, A. S. H., Baltensperger, U. and Slowik, J. G.: On
913 the fate of oxygenated organic molecules in atmospheric aerosol particles, Science Advances,
914 6(11), eaax8922, doi:10.1126/sciadv.aax8922, 2020.

915 Qi, L., Chen, M., Stefenelli, G., Pospisilova, V., Tong, Y., Bertrand, A., Hueglin, C., Ge, X.,
916 Baltensperger, U., Prévôt, A. S. H. and Slowik, J. G.: Organic aerosol source apportionment in

Zurich using an extractive electrospray ionization time-of-flight mass spectrometer (EESI-TOF-MS) – Part 2: Biomass burning influences in winter, Atmos. Chem. Phys., 19(12), 8037–8062, doi:10.5194/acp-19-8037-2019, 2019.

Qi, L., Vogel, A. L., Esmaeilirad, S., Cao, L., Zheng, J., Jaffrezo, J.-L., Fermo, P., Kasper-Giebl, A., Daellenbach, K. R., Chen, M., Ge, X., Baltensperger, U., Prévôt, A. S. H. and Slowik, J. G.: A 1-year characterization of organic aerosol composition and sources using an extractive electrospray ionization time-of-flight mass spectrometer (EESI-TOF), Atmospheric Chemistry and Physics, 20(13), 7875–7893, doi:10.5194/acp-20-7875-2020, 2020.

Slowik, J. G., Stainken, K., Davidovits, P., Williams, L. R., Jayne, J. T., Kolb, C. E., Worsnop, D. R., Rudich, Y., DeCarlo, P. F. and Jimenez, J. L.: Particle Morphology and Density Characterization by Combined Mobility and Aerodynamic Diameter Measurements. Part 2: Application to Combustion-Generated Soot Aerosols as a Function of Fuel Equivalence Ratio, Aerosol Sci. Technol., 38(12), 1206–1222, doi:10.1080/027868290903916, 2004.

Stefenelli, G., Pospisilova, V., Lopez-Hilfiker, F. D., Daellenbach, K. R., Hüglin, C., Tong, Y., Baltensperger, U., Prévôt, A. S. H. and Slowik, J. G.: Organic aerosol source apportionment in Zurich using an extractive electrospray ionization time-of-flight mass spectrometer (EESI-TOF-MS)--Part 1: Biogenic influences and day--night chemistry in summer, Atmos. Chem. Phys., 19(23), 14825–14848 [online] Available from: https://acp.copernicus.org/articles/19/14825/2019/, 2019.

Sueper, D.: ToF-AMS Data Analysis Software Webpage, [online] Available from: http://cires1.colorado.edu/jimenez-group/wiki/index.php/ ToF-AMS_Analysis_Software (Accessed 13 April 2023), 2023.

Tennison, S. R.: Phenolic-resin-derived activated carbons, Appl. Catal. A, 173(2), 289–311, doi:10.1016/S0926-860X(98)00186-0, 1998.

Tong, Y., Qi, L., Stefenelli, G., Wang, D. S., Canonaco, F., Baltensperger, U., Prévôt, A. S. H. and Slowik, J. G.: Quantification of primary and secondary organic aerosol sources by combined factor analysis of extractive electrospray ionisation and aerosol mass spectrometer measurements (EESI-TOF and AMS), Atmospheric Measurement Techniques, 15(24), 7265–7291, doi:10.5194/amt-15-7265-2022, 2022.

Ulbrich, I. M., Canagaratna, M. R., Zhang, Q., Worsnop, D. R. and Jimenez, J. L.: Interpretation of organic components from positive matrix factorization of aerosol mass spectrometric data, Atmospheric Chemistry & Physics, 9(9) [online] Available from: https://d-nb.info/114970523X/34, 2009.

Ulbrich, I. M., Handschy, A. V., Lechner, M. and Jimenez, J. L.: High-Resolution AMS Spectral Database, [online] Available from: http://cires.colorado.edu/jimenez-group/HRAMSsd/, 2019.

Wang, D. S., Lee, C. P., Krechmer, J. E., Majluf, F., Tong, Y., Canagaratna, M. R., Schmale, J., Prévôt, A. S. H., Baltensperger, U., Dommen, J., El Haddad, I., Slowik, J. G. and Bell, D. M.: Constraining the response factors of an extractive electrospray ionization mass spectrometer for

near-molecular aerosol speciation, Atmos. Meas. Tech., 14(11), 6955–6972, doi:10.5194/amt-14-6955-2021, 2021.

Xu, W., Lambe, A., Silva, P., Hu, W., Onasch, T., Williams, L., Croteau, P., Zhang, X., Renbaum-Wolff, L., Fortner, E., Jimenez, J. L., Jayne, J., Worsnop, D. and Canagaratna, M.: Laboratory evaluation of species-dependent relative ionization efficiencies in the Aerodyne Aerosol Mass Spectrometer, Aerosol Sci. Technol., 52(6), 626–641, doi:10.1080/02786826.2018.1439570, 2018.

Zhang, Q., Alfarra, M. R., Worsnop, D. R., Allan, J. D., Coe, H., Canagaratna, M. R. and Jimenez, J. L.: Deconvolution and quantification of hydrocarbon-like and oxygenated organic aerosols based on aerosol mass spectrometry, Environ. Sci. Technol., 39(13), 4938–4952, doi:10.1021/es048568l, 2005.

Zhang, Q., Jimenez, J. L., Canagaratna, M. R., Allan, J. D., Coe, H., Ulbrich, I., Alfarra, M. R., Takami, A., Middlebrook, A. M., Sun, Y. L., Dzepina, K., Dunlea, E., Docherty, K., DeCarlo, P. F., Salcedo, D., Onasch, T., Jayne, J. T., Miyoshi, T., Shimono, A., Hatakeyama, S., Takegawa, N., Kondo, Y., Schneider, J., Drewnick, F., Borrmann, S., Weimer, S., Demerjian, K., Williams, P., Bower, K., Bahreini, R., Cottrell, L., Griffin, R. J., Rautiainen, J., Sun, J. Y., Zhang, Y. M. and Worsnop, D. R.: Ubiquity and dominance of oxygenated species in organic aerosols in anthropogenically-influenced Northern Hemisphere midlatitudes, Geophys. Res. Lett., 34(13), doi:10.1029/2007gl029979, 2007.

Zhang, Y., Williams, B. J., Goldstein, A. H., Docherty, K., Ulbrich, I. M. and Jimenez, J. L.: A Technique for Rapid Gas Chromatography Analysis Applied to Ambient Organic Aerosol Measurements from the Thermal Desorption Aerosol Gas Chromatograph (TAG), Aerosol Sci. Technol., 48(11), 1166–1182, doi:10.1080/02786826.2014.967832, 2014.

Zhang, Y., Williams, B. J., Goldstein, A. H., Docherty, K. S. and Jimenez, J. L.: A technique for rapid source apportionment applied to ambient organic aerosol measurements from a thermal desorption aerosol gas chromatograph (TAG), Atmospheric Measurement Techniques, 9(11), 5637–5653, doi:10.5194/amt-9-5637-2016, 2016.

Supporting information for:

"A multi-instrumental approach for calibrating two real-time mass spectrometers using high performance liquid chromatography and positive matrix factorization"

Melinda K. Schueneman[1], Douglas A. Day[1], Dongwook Kim[1], Pedro Campuzano-Jost[1], Seonsik Yun[1], Marla P. DeVault[1], Anna C. Ziola[1], Paul J. Ziemann[1], and Jose L. Jimenez[1]

[1]Department of Chemistry and Cooperative Institute for Research in Environmental Sciences, University of Colorado, Boulder, CO 80309, USA

S1 General system information for multi-instrumental calibration method

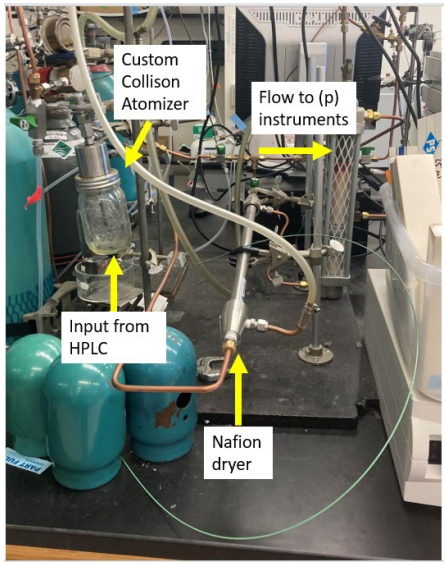

Figure S1. HPLC tubing into custom atomizer

Table S1. Tube volumes, flows, and residence times from HPLC separation to particle instrument detection.

Item	Total volume (mL)	Flow rate (flow through)	Residence time
Tubing transferring liquid from after HPLC column and UV-Vis detection to atomizer	0.67	1.0 mL min^{-1}	40 s
Atomizer	500	8.0-10 ~~l~~L min^{-1}	3.0 - 3.~~75~~ 8 s
Nafion drier	7.0	~ 8.0 ~~l~~L min^{-1}	0.053 s
Tubing before manifold	1~~1~~208~~.3~~	7.2 ~~l~~L min^{-1}	1.0 s
Post manifold EESI	31~~.2~~	0.84 ~~l~~L min^{-1}	2.2 s
Post manifold AMS	14~~.1~~	1.5 ~~l~~L min^{-1}	0.60 s

Formatted: Font: 10 pt

Formatted: Font: 10 pt

Post manifold SMPS A	34.2	1.43 l L min^{-1}	1.4 s
Post manifold SMPS B	28.59	1.49 L l min^{-1}	1.2 s

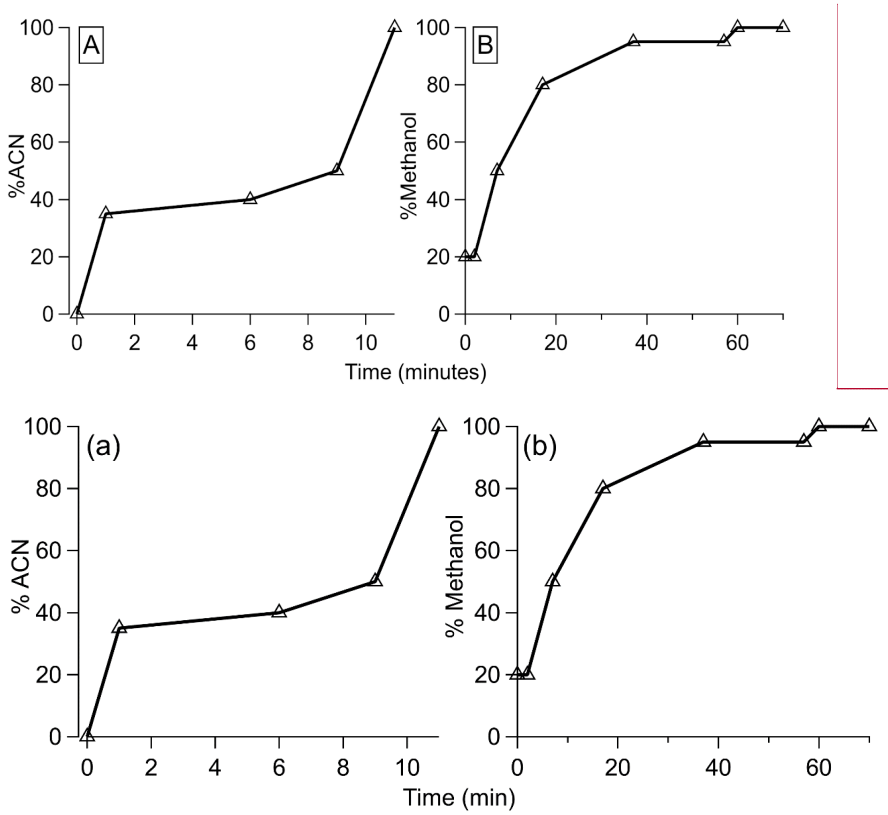

Figure S2. Solvent gradients for (Aa) standard HPLC runs and (Bb) β-pinene HPLC run. The other solvent was a mixture of 95 % H_2O / 5 % ACN.

Commented [P1]: Deleted image, reformatted

Formatted: Font: 10 pt

Formatted: Font: 10 pt

Formatted: Font: 10 pt

Table S2. Standard compounds used for HPLC method demonstration, source and purity, volatility (calculated using published vapor pressures), estimated percent evaporated during transmission (from atomizer output to detection, calculated with C^* and measured OA concentration at detection), and density (using the ratio of d_{va}/d_m)

Species	Source + purity	Saturation Mass Concentration (µg m^{-3}) (T=298 K)	Estimated Percent Evaporated	Density
3-methyl-4-nitrophenol	Aldrich, 98 %	5,210	92 %	1.27**
Phthalic acid	Beantown Chemical, ACS grade, 99.5 %	5.72	0 %	1.05
4-nitrophenol	Aldrich, 99 %	10,600	94 %	1.48**
Succinic acid	Aldrich, 99 %	1.21	0 %	1.18
4-nitrocatechol	Alfa Aesar, 98 %	64	63 %	1.26
L-malic acid	Aldrich, 97 %	0.24	-	1.28
Citric acid	Fisher Scientific	0.18	-	-
Levoglucosan	Chem-Impex Int'l, ≥ 99.0 %	13*	-	1.30
Acetonitrile	Fisher Chemical, > 99.95 %	-	-	-
Methanol	Fisher Chemical, > 99.9 %	-	-	-
Water	VWR Chemicals, HPLC grade	-	-	-
Ethyl Acetate	Fisher Chemical, 99.5 %	-	-	-

***Reported in (Pagonis et al., 2021)**

****Density of bulk solution from literature**

Formatted: Font: 10 pt

Formatted: Font: 10 pt, Superscript

Formatted: Font: 10 pt

Formatted Table

Formatted: Font: 10 pt

Formatted: Font: 10 pt

Formatted: Font: 10 pt

The densities measured using the d_{va}/d_m ratio do not match the literature values for bulk density well. This is potentially due to different phases from that of the bulk material, and/or non-spherical particle shape (Jayne et al., 2000; Huffman et al., 2005). Regardless, the d_{va}/d_m density was used as the best estimate here.

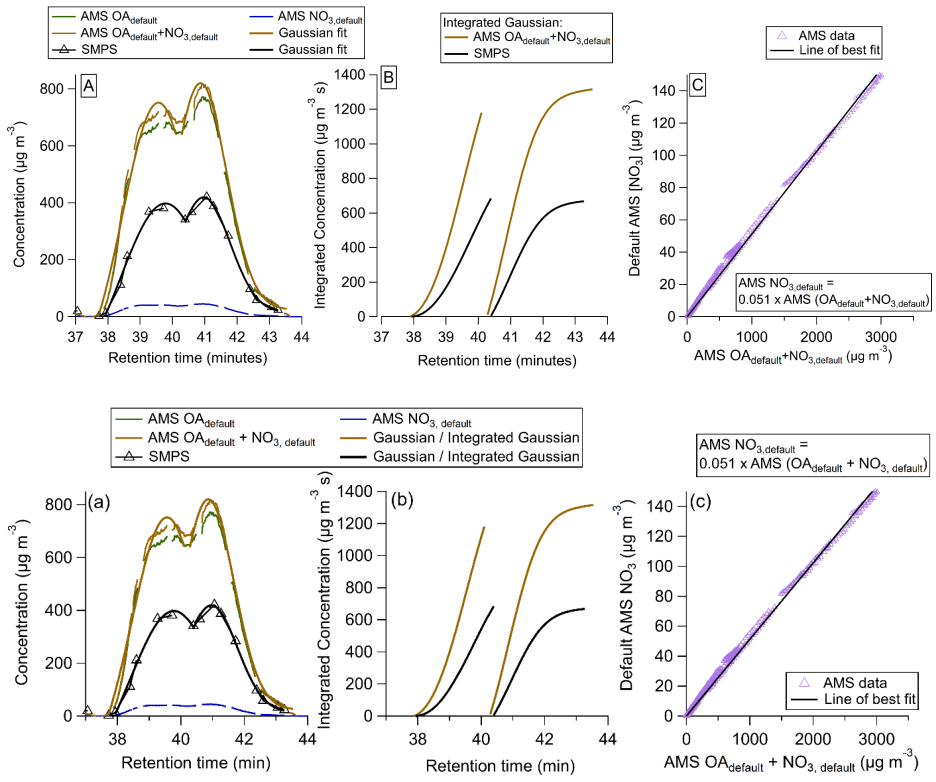

Figure S3. (~~A~~a) AMS default mass concentrations for [OA], [NO_3], and [OA + NO_3]; SMPS mass concentrations, corrected for the average density. (~~B~~b) Integrated Gaussian curves for each peak. (~~C~~c) Default AMS [NO_3] vs total default AMS signal [OA + NO_3], fit with a line. The slope (ratio of [NO_3]/[OA + NO_3]) = 0.051.

The nitrate contribution to the total mass for this peak was ~5.1 %. Fitting the bulk peaks (which are composed of multiple eluents) may result in some error in the nitrate contribution approximation. CF_x^A was calculated for the two

Formatted: Font: 10 pt

Commented [P2]: Deleted image, reformatted

Formatted: Font: 10 pt

Formatted: Font: 10 pt

Formatted: Font: 10 pt

Formatted: Font: 10 pt

Formatted: Font: 10 pt

Formatted: Font: 10 pt

peaks by referencing the AMS mass to the SMPS mass. For the first peak, CF_x^A = 1.97, for the second peak CF_x^A = 1.73.

S2 SMPS testing and validation

S2.1 Fast scanning operation and validation

The fast scanning operation of the SMPSs was essential here. A "fast scan" here means 30 seconds for voltage scanning, with 10 seconds retrace time (when the voltage is returned back to 0). This allows for an SMPS data point to be obtained every 40 seconds, and when two SMPSs are used with interleaved timing, every ~ 20 seconds. This faster scanning is not without precedent; one paper published in 1990 first denoted the term "scanning electrical mobility spectrometer" or SEMS (Wang and Flagan, 1990). In that paper, researchers demonstrated that aerosol distributions for atmospherically relevant samples could be measured in a 30 -second scan time, with a 30- second s retrace time. This research led to the creation of new SMPSs that, like the SEMS, scanned continuously, and thus would be capable of 30 s scanning times. A study a few years later put this to the test, and looked at the impact of changing SMPS scan times, and found that shorter scan times led to more smearing (less-resolved size distributions) and lower peak maximas (Russell et al., 1995). They suggest that this is driven by the residence time of the particles from the output of the DMA to the optical detection by the CPC (t_d). In addition, a paper in 2002 elaborated on the conclusions from Russell et. al. (1995), and found that when scanning with a flow rate of 0.3 Ll min^{-1}, combined with a 30 seconds scan time, the size distribution was significantly broadened (Collins et al., 2002). The maximum concentration was decreased by over 50 % when compared to a longer scan time (300 s), but the integrated concentration did not seem as affected, due to broadening in the faster scan.

Typically, SMPSs are run at longer scan times of two 2 minutes or more (Sioutas, 1999; McMurry, 2000; Jeong and Evans, 2009). One study modified an SMPS by adding an aerosol particle mass analyzer (APM). With the modified system, data points were recorded every 60 seconds (Malloy et al., 2009). Another study, which took place on an aircraft and measured the air over Mexico City, ran their SMPS with a scan time of 1.5 minutes (DeCarlo et al., 2008). Despite the conclusions of Wang and Flagan (1990), many in the community run their SMPSs as "slow" (e.g. scan times of two or more minutes) instruments. Henceforth, "slow" will refer to the 2 minute scans, and "fast" will refer to the 30 second scans.

Here, we test each SMPS with a combination of "long" scans (2- minute scans, 15 s retrace, 3 l L min^{-1} sheath flow) and "fast" scans (30 s scans, 10 s retrace, 6 l L min^{-1} sheath flow). In order to assess the usability and accuracy of the fast scan method, tests were carried out (Fig. S4) to compare the total integrated volume concentration, number size distributions, and volume size distributions for 2two minute min scans at both a sample flow of 0.3 l L min^{-1} and 1.5 Ll min^{-1}, and 30 second scans done with the same flow rates.

Formatted: Font: 10 pt

Formatted: Font: 10 pt

Formatted: Font: Italic

Formatted: Font: 10 pt

Formatted: Font: 10 pt

Formatted: Font: 10 pt

Formatted: Font: 10 pt

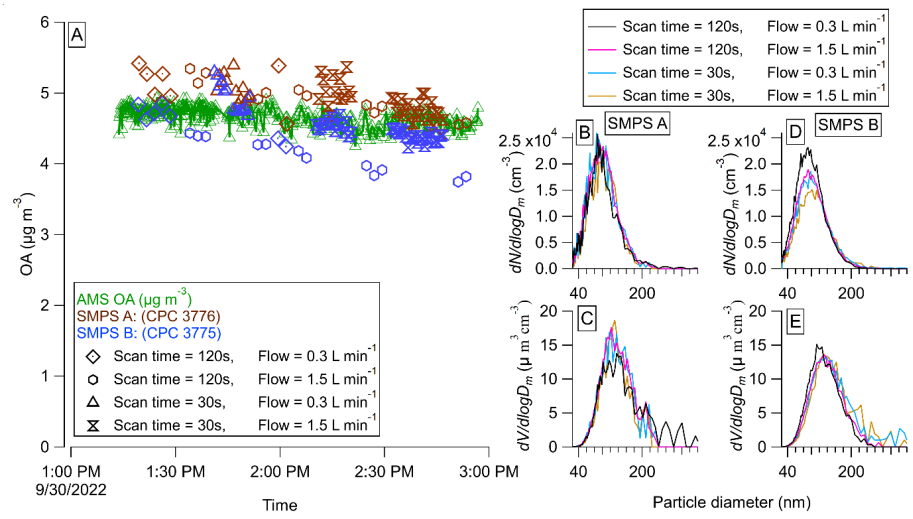

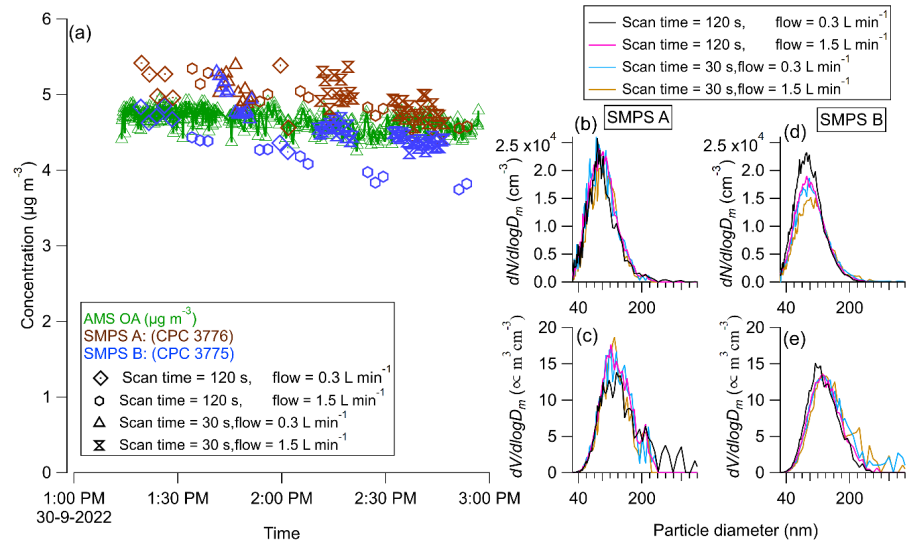

Figure S4. (~~A~~a) Estimated particle mass concentration from SMPS A and B compared to the total OA measured by the AMS, for different combinations of scanning times and sample flow rates when sampling constant DOS concentrations from a large chamber. (~~B~~b) Number distribution comparisons for different combinations of scanning times and flow rates for SMPS A, (~~C~~c) Volume distribution comparisons, (~~D~~d) number distribution comparisons for SMPS B, and (~~E~~e) volume distribution comparisons for SMPS B.

Commented [P3]: Deleted image, reformatted below

Formatted: Font: 10 pt

Formatted: Font: 10 pt

Formatted: Font: 10 pt

Formatted: Font: 10 pt

Formatted: Font: 10 pt

Formatted: Font: 10 pt

In Fig. S4a, the total concentration of dioctyl sebacate (DOS) was measured by an AMS (green) and time averaged to 10 seconds. The AMS- measured DOS (after AMS calibration for that species) was used as the reference concentration. DOS was generated using a custom evaporation-condensation apparatus (Sinclair and La Mer, 1949; Krechmer et al., 2017)(Sinclair and La Mer, 1949), and flowed into a 20 m^3 Teflon chamber. To start, we scanned with both SMPSs set to a 2 minute scan time with a 15 second retrace time, and a flow rate of 0.3 L l min^{-1}. This is typically how we run our SMPSs for laboratory studies and we have compared with even longer scans (up to 300 s, same flow settings) showing good agreement (Liu et al., 2019) and has shown good quantitative agreement for intercomparisons during chamber and field campaigns. Those "long scans" serve as a reference. Both SMPSs were run concurrently.

Some researchers show peak smearing when using faster scan times (although, those studies seem to use a sample flow rate=0.3 l L min^{-1}) (Russell et al., 1995). These studies posit that the smearing is mainly due to instrument specific/plumbing delay times from the output of the DMA to the optical detection by the CPC (Russell et al., 1995). In Fig. S4b, the number distribution is shown for the different flow / scan time configurations for the SMPS A. The black distribution for all scans is the reference (120 s scan, 0.3 l L min^{-1}, resolution=10). For the number distribution, the peak width for the reference is more narrow than for all other configurations. The difference is minor, however, and not as large as in other reports.

In Fig. S4c, the volume distributions are compared. The reference scan has a lower maximum concentration than the other configurations, which seems to go against previously published results. Over time, [DOS] measured by the AMS decreases, due to chamber wall loss effects. To counter this, reference scans (120 scans, 0.3 l L min^{-1} flows) are carried out throughout the experiment. For reference, the SMPSs were run with 30 s scans and 1.5 l L min^{-1} sample flows for the HPLC method proposed in the main text.

The distributions for SMPS B are more affected by the different configurations. This is unsurprising, as it has a longer t_d than SMPS A (table S3), and likely is more representative of the systems studied in the research cited above. In Fig. S4d, the number distribution for the reference scan has a higher maximaa higher maximum than the other scans. The faster, high flow scan is the most different from the reference, and has both a lower maxima and a wider peak width (resolution = 4). This matches previous findings (Collins et al., 2002), but this study shows a far less dramatic peak shape difference than that shown therein. This finding could introduce some quantification error. In Fig. S4, the volume distributions match fairly well for all configurations. A faster instrument (such as an optical particle counter) would be ideal to obtain faster measurements, but the small diameter particles produced by the Collison atomizer makes running those instruments impractical and prone to error (due to low detection efficiency at smaller size particles).

For the multi-instrumental calibration experiments, SMPS A and SMPS B were offset by twenty 20 seconds. That allowed us to obtain a volume concentration every approx. 20 seconds. For comparing the response between the two SMPSs, an experiment was done where SMPS A and SMPS B were run concurrently (Fig. S5).

Formatted: Font: 10 pt

Formatted: Font: 10 pt

Formatted: Font: 10 pt

Formatted: Font: 10 pt

Formatted: Font: 10 pt

SMPS A and SMPS B are shown to match within ~ 0 % - 10 % (at the maxima). The consistency observed in Fig. S5 between SMPS A and SMPS B provides increased confidence in the use of each instrument in "fast" mode.

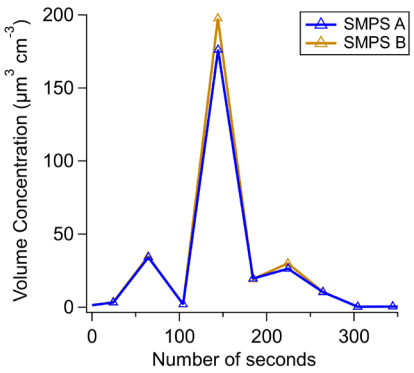

Figure S5. Concurrent SMPS scans for an HPLC run

S2.2 SMPS delay time calculations

Delay times from the aerosol sampling manifold to the DMAs were calculated by running each DMA to size select particles with a mobility diameter of 115 nm. Following transmission, the time it takes for the CPC concentration to reach half of its maximum concentration ($t_{1/2}$) was calculated (table S3). Here, delay times were short, due to the high sample flow. This does not eliminate the importance of having accurate delay times. Fast scans are often prone to more error than their slow counterparts.

To calculate t_d (table S3), polystyrene latex spheres (PSLs) of a known diameter were atomized and measured by the SMPSs. Calculating delay times ($t_{1/2}$ and t_d [delay time from exit of the DMA to the CPC]) allowed us to properly align the slower SMPS measurements with the fast mass spectrometer measurements during the relatively short chromatographically-separated compound peaks. Each eluting HPLC peak is only approx. 1.5 min~~utes~~ long, and the instruments are run at different time resolutions. Each SMPS collects one data point every 40 s~~econds~~. For each data point, the SMPS software provided an uncorrected scanning start time. During the 40- s~~econd~~ scan, concentrations can change significantly. If the SMPS scan starts 15 s~~econds~~ before the maxima is reached, then the scan is recording concentrations at particle diameters both before, during, and after the peak maxima. If the SMPSs were not corrected for their delay times, then the SMPS data point would show an erroneously low / high concentration, and lead to errors when comparing to the other instruments.

Table S3. Delay times for each SMPS. $t_{1/2}$ is the time it takes for the CPC concentration to reach half of its maximum concentration

Formatted: Font: 10 pt

Formatted: Font: 10 pt

Formatted: Font: 10 pt, Italic

Formatted: Font: 10 pt

SMPS name	CPC type	Delay time ($t_{1/2}$) (s)	DMA -> to CPC delay time (t_d) (s)
SMPS A	3776	10.5	0.43
SMPS B	3775	8	1.55

Formatted Table

S3 Standard mixture mass spectra comparison for direct and multi-instrumental calibrations factors

Mass spectra were obtained from PMF for many of the standards used in Sect. 3.2 and compared against the average mass spectra from direct calibrations (Fig. S6).

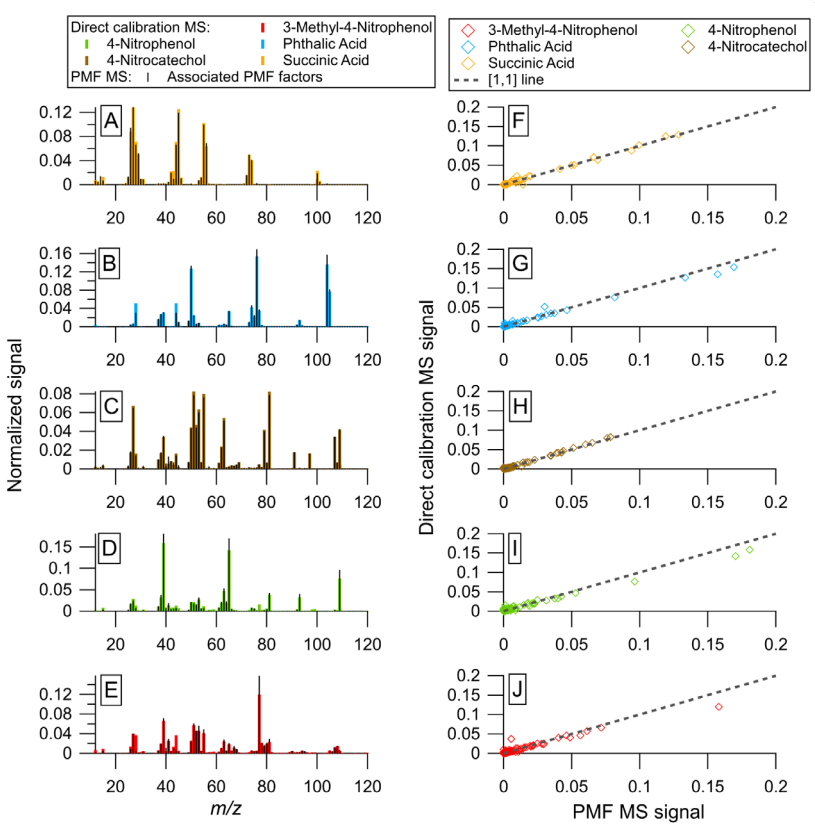

Commented [P4]: Deleted image, reformatted

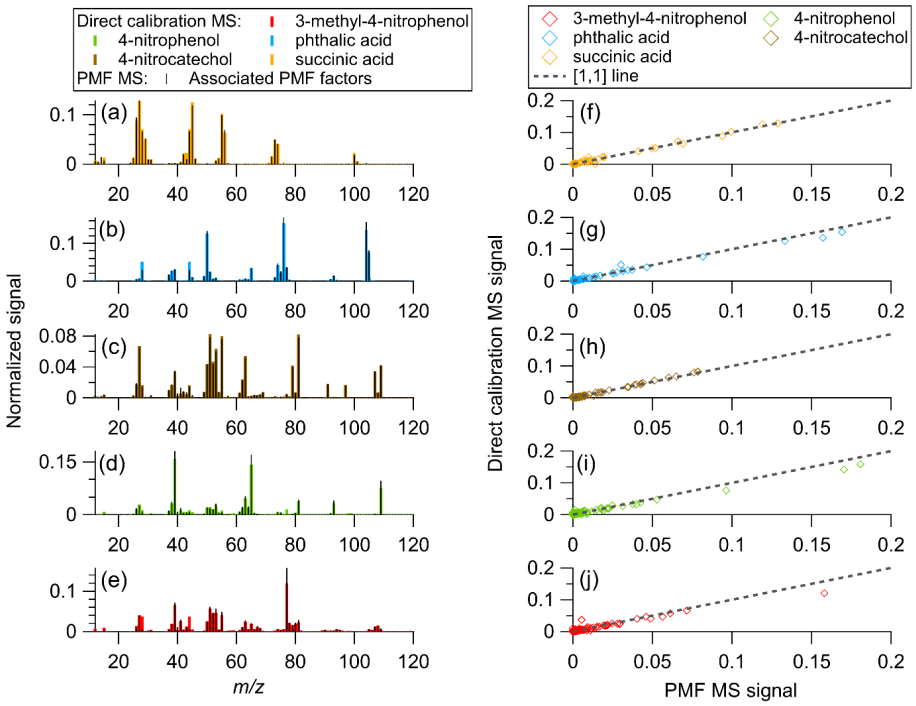

Figure S6. (Aa) - (Ee) Mass spectra for monodisperse calibrations and associated PMF factors for species directly calibrated. (Ff)-(Jj) scatter plot of MS signal at each measured *m/z* for the direct calibrations vs the PMF mass spectra.

The uncentered correlation coefficients (table S4) match well between the assigned PMF factor mass spectra and the corresponding direct calibration mass spectra.

Table S4. Uncentered correlation coefficient (UC) between AMS direct calibration and PMF factor mass spectra (Ulbrich et al., 2009)

	Direct calibration MS				

Formatted: Font: 10 pt

Formatted: Font: 10 pt

Formatted: Font: 10 pt

Formatted: Font: 10 pt

Formatted Table

PMF factor MS	Succinic aAcid	4-Nitrocatechol nitrocatechol	Phthalic Acidacid	4-Nitrophenol nitrophenol	3-methyl-4-nitrophenol
Succinic Acidacid	**0.99**	0.38	0.14	0.15	0.30
Nitrocatechol 4-nitrocatechol	0.38	**1.0**	0.23	0.49	0.62
Phthalic aAcid	0.094	0.20	**0.99**	0.24	0.31
Nitrophenol 5-nitrophenol	0.10	0.43	0.24	**0.99**	0.45
3-methyl-4-nitrophenol	0.21	0.58	0.27	0.49	**0.96**

The UC provides the same information as the dot product, without the need to normalize the mass spectra. For all species, the UC > 0.95. For 4-nitrocatechol, the UC rounded up to 1.0 (near perfect agreement).

Similarly to the process carried out above, the mass spectra from the PMF solution for the data shown in Fig. 6 was compared to direct calibrations (Fig. S7).

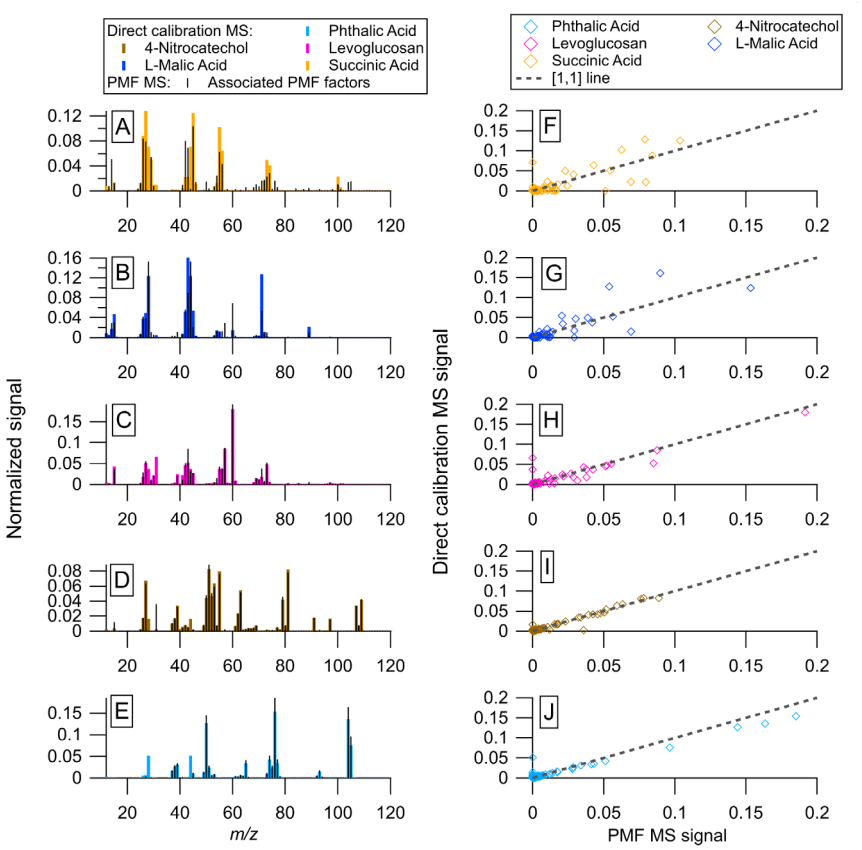

160

Commented [P5]: Deleted image, reformatted

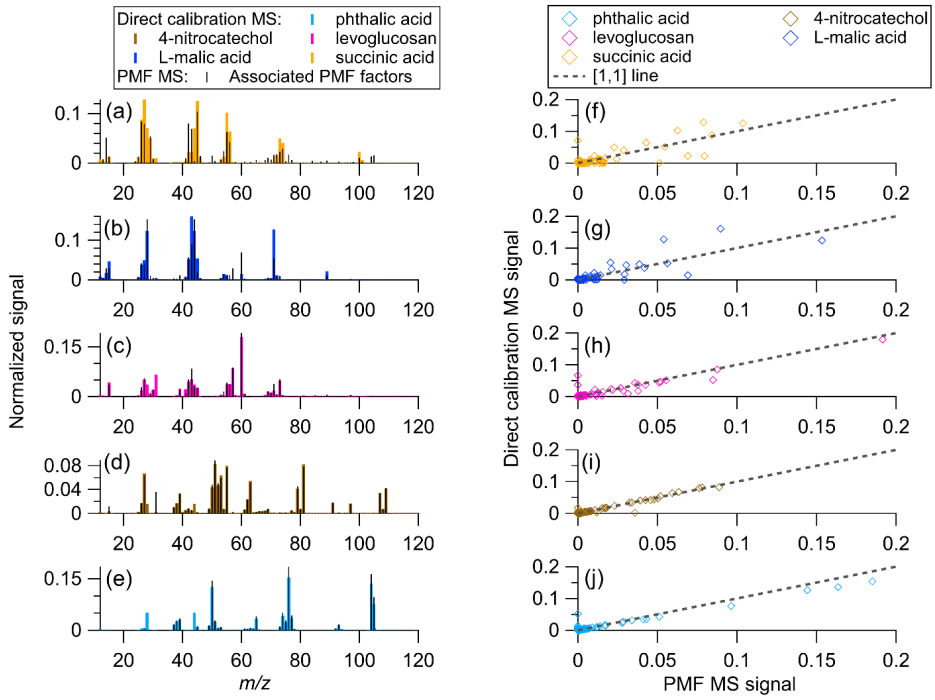

Figure S7. (Aa) - (Ee) Mass spectra for monodisperse calibrations and associated PMF factors for species directly calibrated for the second standard solution (Fig. 6). (Ff) - (Jj) scatter plot of MS signal at each measured *m/z* for the direct calibrations vs the PMF mass spectra.

Formatted: Font: 10 pt

Uncentered correlation coefficients were also calculated (table S5) and generally showed less agreement than those shown in table S4.

Table S5. Uncentered correlation coefficient (UC) between AMS direct calibration and PMF factor mass spectra (Ulbrich et al., 2009) for standard solution 2 (Fig. 6, Fig. S7)

	Direct calibration MS				
PMF factor MS	Succinic ~~Acid~~acid	~~Malic~~ L-malic ~~Acid~~acid	Levoglucosan	4-~~N~~nitrocatechol	Phthalic ~~Acid~~acid
Succinic ~~Acid~~ acid~~PMF~~	**0.81**	0.50	0.35	0.31	0.17
~~Malic~~ L-malic ~~A~~acid ~~PMF~~	0.55	**0.89**	0.60	0.20	0.23
Levoglucosan ~~PMF~~	0.36	0.41	**0.93**	0.19	0.029
~~Nitrocatechol~~ 4-nitrocatechol ~~PMF~~	0.33	0.12	0.23	**0.98**	0.20
Phthalic ~~Acid~~ acid~~PMF~~	0.030	0.014	0.025	0.19	**0.96**

Levoglucosan, 4-nitrocatechol, and phthalic acid match well (UC > 0.9). Succinic acid and L-malic acid match less well, but still have a UC > 0.8. As expected, the UC's for the second standard solution are less good than those for the first standard solution (which was almost entirely resolved even without PMF).

Formatted: Font: 10 pt
Formatted: Font: 10 pt
Formatted: Font: 10 pt
Formatted: Line spacing: single
Formatted Table
Formatted: Line spacing: single
Formatted: Line spacing: single
Formatted: Line spacing: single
Formatted: Line spacing: single
Formatted: Line spacing: single

S4 β-pinene detailed information: density, molecular identification, PMF solution, and peak fitting

For the SOA samples, the effective density was calculated as described in Sect. 2.5.2, shown in Fig. S8.

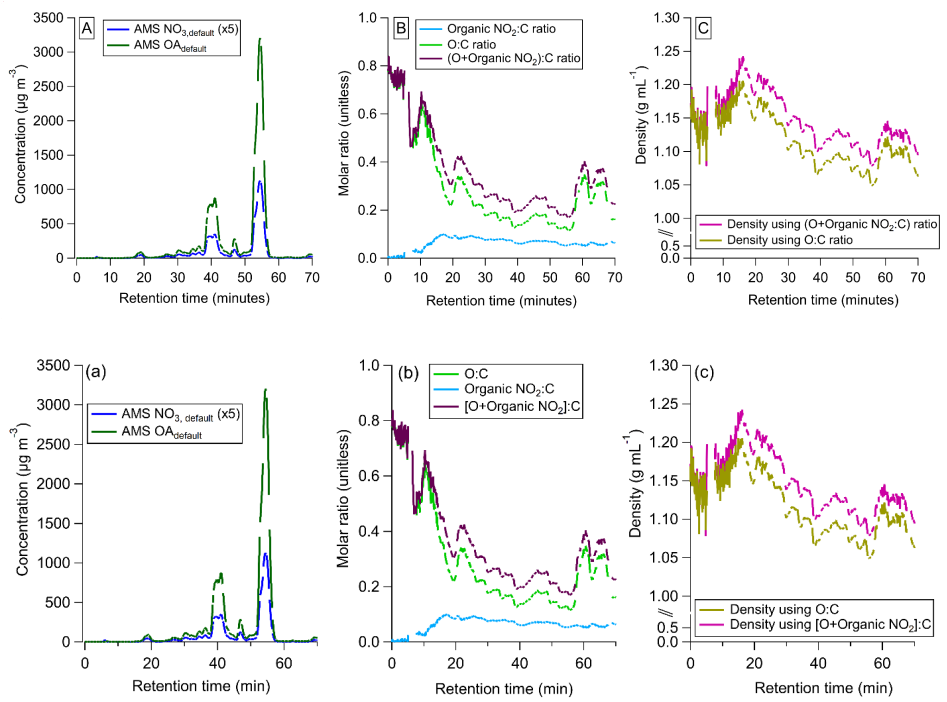

Figure S8. (~~A~~a) Measured NO_3 and OA from the AMS when sampling β-pinene + NO_3 SOA. (~~B~~b) Atomic ratios for organic nitrate : carbon, oxygen to carbon, and oxygen + organonitrates to carbon. (~~C~~c) Estimated density from two approaches.

The chromatogram from Claflin and Ziemann (2018) was compared to that measured here (Fig. 7), shown below in Fig. S9.

Commented [P6]: Deleted image, reformatted

Formatted: Font: 10 pt

Formatted: Font: 10 pt

Formatted: Font: 10 pt

Formatted: Font: 10 pt

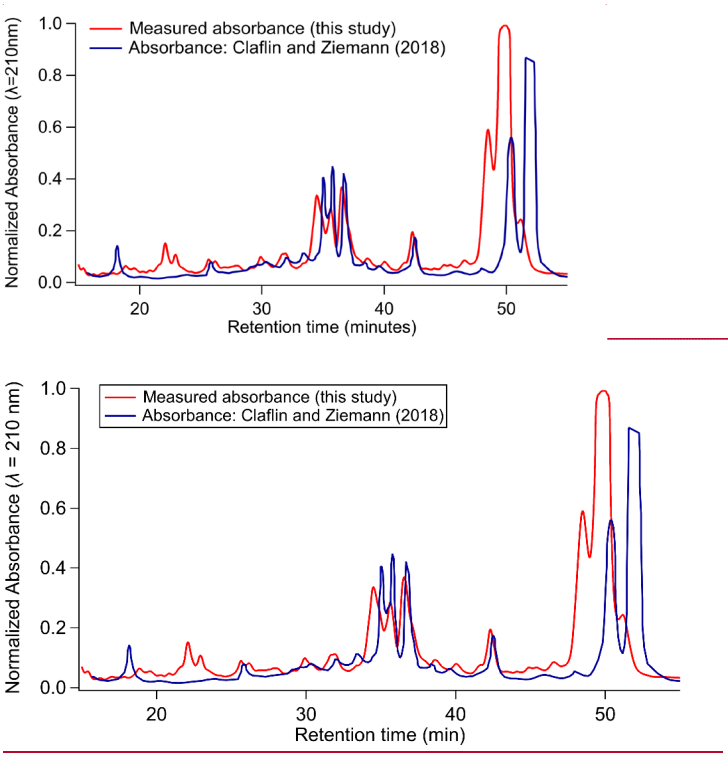

Figure S9. Comparison to β-pinene + NO_3 SOA chromatogram measured in Claflin and Ziemann (2018).

The chromatograms show the same general shape, although with slightly faster elution for this work. There are some notable differences in the results between 20 - 30 min~~utes~~ and 45 - 55 min~~utes~~. The final peak in the chromatogram from Claflin and Ziemann is the same peak as the largest one measured here (retention time ~ 50 min~~utes~~). This suggests that there could be some difference in the HPLC gradient method, or a potential contamination in one of the HPLC solvents. Despite that, the overall signals are consistent, and some of the identified species are shown in table S6.

Table S6. Structure of some known species (from Claflin and Ziemann (2018)), exact (theoretical) mass, observed mass (measured with EESI+), and mass accuracy (based on EESI instrument multi-ion *m/z*

Commented [P7]: Deleted image, reformatted

Formatted: Font: 10 pt

Formatted: Font: 10 pt

Formatted: Font: 10 pt

Formatted: Font: 10 pt

Formatted: Font: 10 pt

Formatted: Font: 10 pt

calibration fit).

Structure	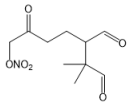	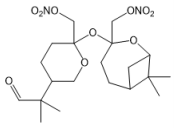	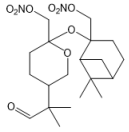	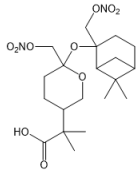	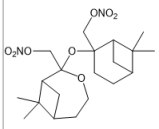
MW	245.23	460.48	444.48	460.48	428.48
Exact mass (+Na^+) (Da)	268.0797	483.1955	467.2002	483.1955	451.2056
Detected mass (Da)	268.0879	483.1885	467.2032	483.1885	451.2120
Mass Accuracy (ppm)	30.6	-14.5	6.42	-14.5	14.2

PMF was run on the AMS data, shown below for the entire HPLC run (Fig. S10).

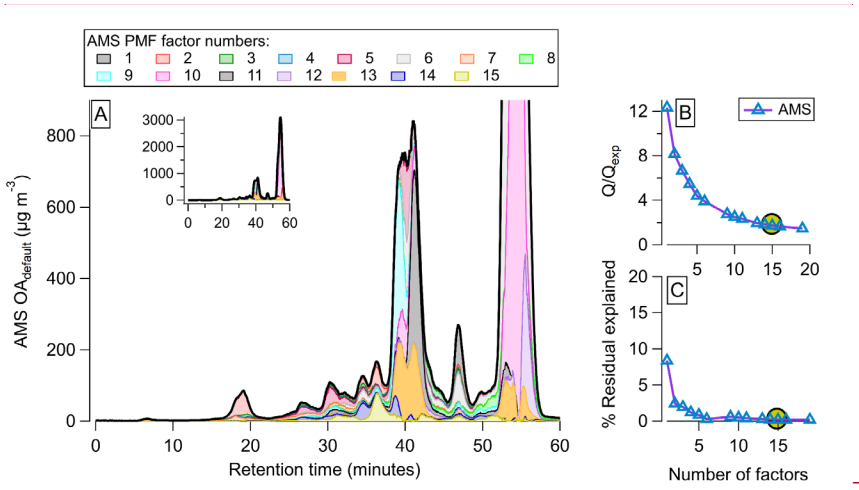

Commented [P8]: Deleted image, reformatted

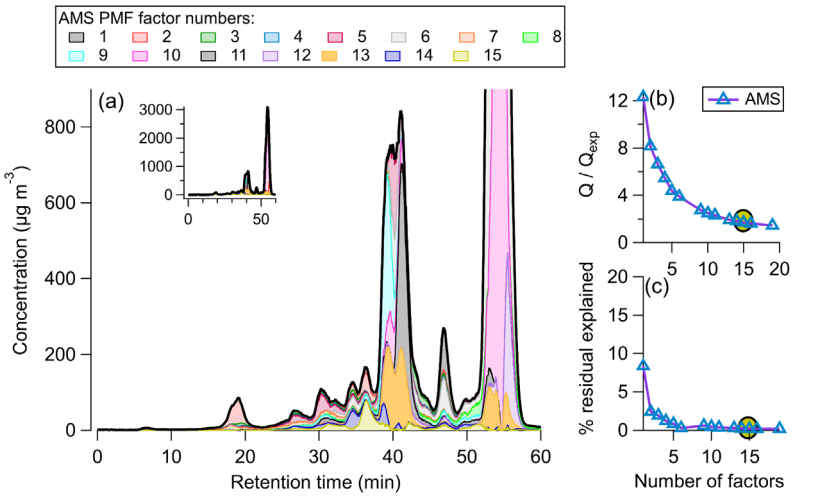

Figure S10. (~~A~~a) stacked plot showing AMS PMF solution time series for the β-pinene~~/~~ + NO_3 SOA system, with inset showing full scale. (~~B~~b) Q / $Q_{expected}$, with the chosen solution (15 factors) circled. (~~C~~c) Percent of the total sum of the residuals explained, 15 factor solution circled.

A 15 factor solution was chosen. The time series and mass spectra for each factor are shown in Fig. S11. The AMS signal during the β-pinene + NO3 HPLC experiment was high, ranging from ~ 100 - 4000 µg m^{-3}. For low volatility species, these high concentrations are not necessary. However, in many systems, the volatility of the produced products will range many orders of magnitude in C^*. To best calibrate for low-volatility and semi-volatile products, higher concentrations of SOA should be injected into the column. For the β-pinene+NO_3 SOA that was shown here, the chamber experiment (as discussed in Claflin and Ziemann, 2018), started with the addition of ~ 200 µg m^{-3} ammonium sulfate seed, 1 ppm of β-pinene, and 0.3 ppm N_2O_5 (in an 8.0 m^3 Teflon FEP chamber). All of the N_2O_5 was reacted, meaning ~ 0.3 ppm of β-pinene was reacted. The amount of SOA formed can be calculated using the known SOA yields, concentrations, and flow rates.

First, 0.3 ppm β-pinene is converted into a mass concentration. Following this step, the mass concentration is multiplied by the known SOA yield (Eq. S1)

$$SOA\ yield = \frac{\Delta SOA}{\Delta VOC} \quad \text{Eq. S1}$$

The SOA yield for this system ranges from ~ 27- ~ 105 % (Boyd et al. 2015). If 30 % of the β-pinene reacted, then the amount of SOA was formed ranged from 372 µg m^{-3} to 1378 µg m^{-3}. This concentration of aerosol was then collected on a filter at a flow rate of 14 L min^{-1} for 120 min. This would imply that 625 µg - 2315 µg of SOA was

Formatted: Font: 10 pt
Formatted: Font: 10 pt
Formatted: Font: 10 pt
Formatted: Font: 10 pt
Formatted: Superscript
Formatted: Superscript
Formatted: Subscript
Formatted: Superscript
Formatted: Subscript
Formatted: Subscript
Formatted: Superscript
Formatted: Subscript
Formatted: Subscript
Field Code Changed
Formatted: Superscript
Formatted: Superscript
Formatted: Superscript

collected on the filter. Assuming a 100 % extraction efficiency of SOA, the amount of material injected into the column can be quantified as such (Eq. S2)

$$Injected\ mass = \frac{mass\ SOA}{volume\ ACN} \times injected\ volume\ of\ solution \quad \text{Eq. S2}$$

A typical volume of acetonitrile (ACN) used would be ~ 2 mL, therefore the concentration of SOA in ACN would range from 313 µg mL^{-1} - 1158 µg mL^{-1}. The maximum injected volume is 50 µL, therefore the total injected mass ranges from 16 µg - 58 µg.

To confirm these results, we use the largest peak in the chromatogram (*m/z* 451.2, retention time ~ 55 min) in an example. According to Claflin and Ziemann (2018), this peak is responsible for ~ 55 % of the total SOA in this system. Therefore, anywhere from 8.8 µg - 32 µg of the injected mass comes from that peak. However, only 0.55 % of that mass makes it to the instruments, so the instruments should observe 0.048 - 0.18 µg.

The observed AMS mass concentration was roughly 2000 µg m^{-3} using the corrected CF_x^A. If we assume the peak is a triangle, we can estimate the area by multiplying the observed peak mass concentration by the total peak elution time (~ 2 min on average) and dividing by 2. This value is 2000 µg m^{-3} × min. The AMS flow was ~ 0.1 L min^{-1} or 1×10^{-4} m^3 min, so the AMS sampled ~ 0.2 µg, which is very close to the 0.18 µg estimated above.

These injected solution concentrations were able to produce the AMS concentrations observed in Fig. 7, Fig. S8, Fig. S10, and Fig. S12. For species with a volatility (C^*) > 100 µg m^{-3}, there would be substantial evaporation, > 50 % at equilibrium. While some evaporation would occur for species with a volatility < 100 µg m^{-3}, like 4-nitrocatechol in Fig. 4, the SMPS, AMS, and EESI seem to mostly agree.

It should be noted that, in our setup, < 1 % of the injected mass made it to the mass spectrometers. The use of the collected sample could be optimized further, allowing the analysis of smaller amounts of mass by this method.

Formatted: Superscript

Formatted: Indent: First line: 0.5"

Formatted: Font: Italic

Formatted: Superscript

Formatted: Superscript

Formatted: Superscript

Formatted: Superscript

Formatted: Superscript

Formatted: Superscript

Formatted: Superscript

Formatted: Superscript

Formatted: Indent: First line: 0.5"

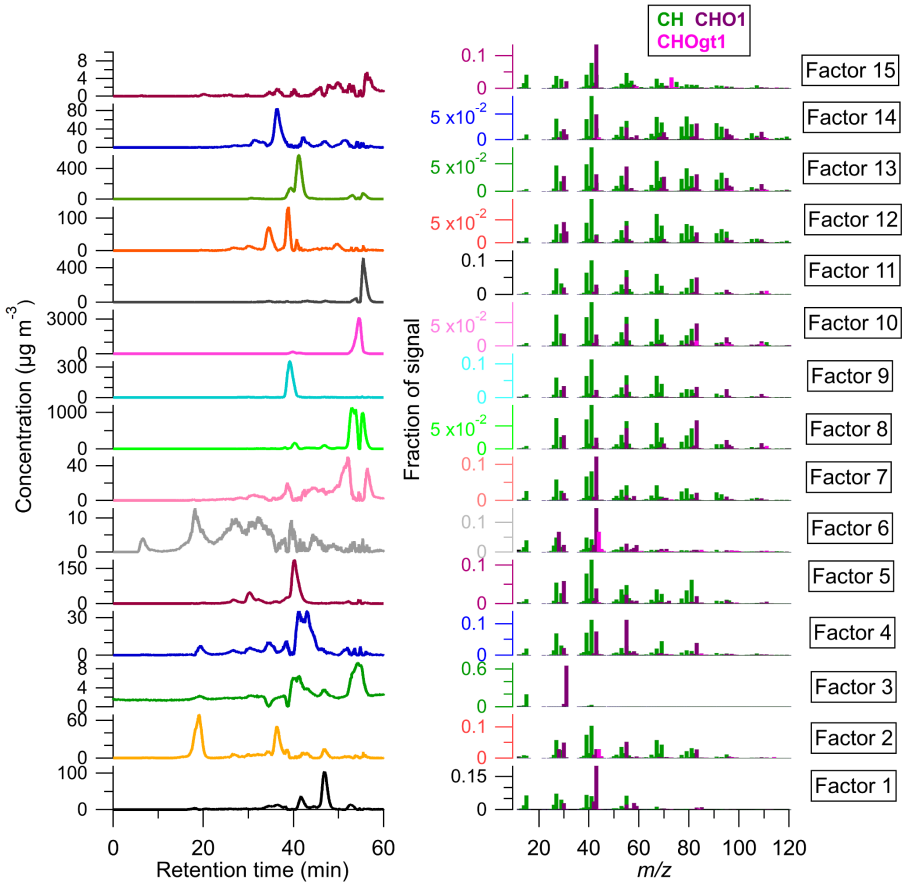
CH CHO1
CHOgt1
Concentration (µg m-3)
Retention time (min)
Fraction of signal
m/z
Factor 15
Factor 14
Factor 13
Factor 12
Factor 11
Factor 10
Factor 9
Factor 8
Factor 7
Factor 6
Factor 5
Factor 4
Factor 3
Factor 2
Factor 1

246

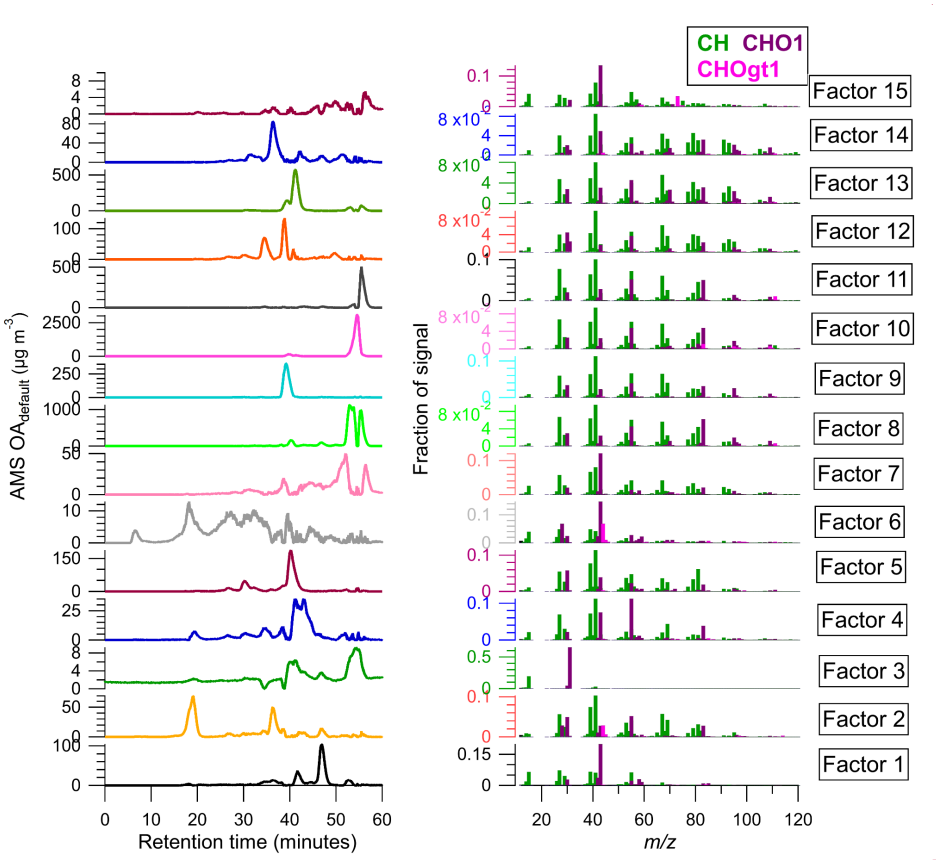

Figure S11. (Left) time series of individual PMF factors for the β-pinene + NO_3 SOA system and (right) HR mass spectra (colored by family) for each factor.

Many of the factors have different time series but very similar mass spectra. This suggests that the species fragment similarly in the AMS (and likely have similar phase states). The SOA products are mostly hydrocarbons with polar moieties (nitrate, carboxylic acids, ketones, and cyclic ethers). Many of the species retained the nonpolar moiety from injection to detection (as shown in the CH dominated mass spectra).

The peaks eluting from ~35 - ~43 minutes showed the strongest overlap (and also contained many of the known β-pinene + NO_3 SOA products). The time series for this portion of the HPLC run is shown in Fig. S12.

Commented [P9]: Deleted image, reformatted

Formatted: Font: 10 pt

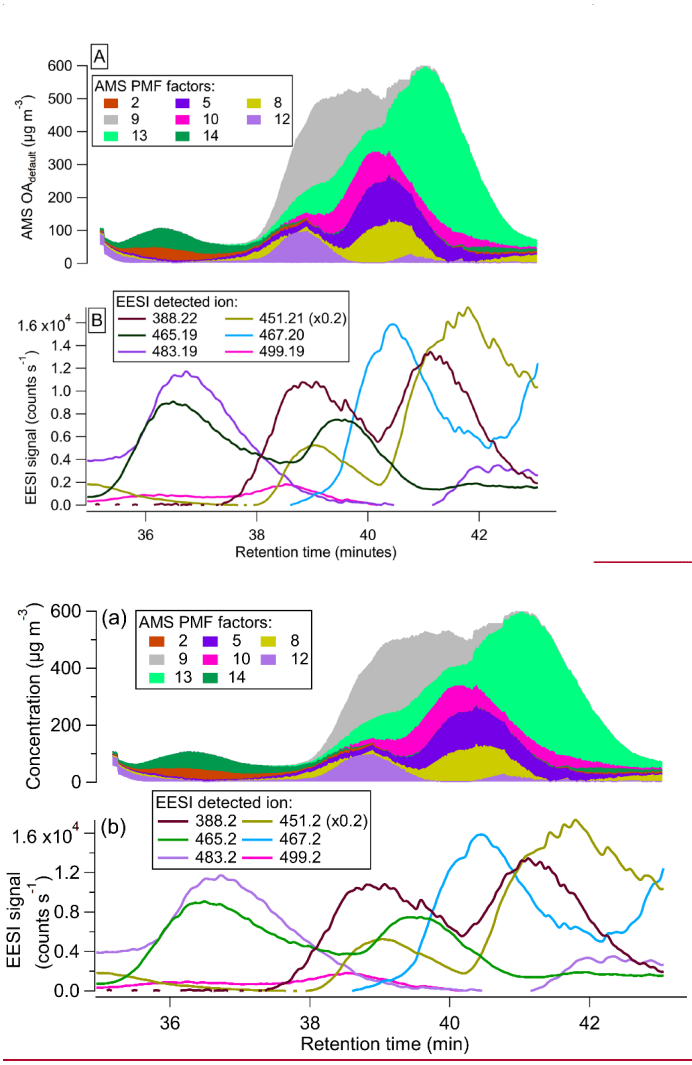

Figure S12. (aA) stacked plot of AMS PMF factors from 35 - 43 minutes and (bB) EESI HR ions time series.

As described in Sect. 3.3, EESI HR ions were matched to AMS PMF factors using the shape of the time series' as well as the retention times. The EESI HR ions and associated AMS PMF factors are shown in Table S7.

Commented [P10]: Deleted image, reformatted

Formatted: Font: 10 pt

Formatted: Font: 10 pt

Formatted: Font: 10 pt

Table S7. EESI HR ion and corresponding AMS PMF factor(s)

EESI HR ion	Associated AMS PMF factor(s)
268.1	-
388.2	9, 13
451.2 (1)	13
451.2 (2)	13
451.2 (3)	-
465.2 (1)	2
465.2 (2)	10
467.2	5,8
483.2	14

Individual peaks are shown in Fig. S13.

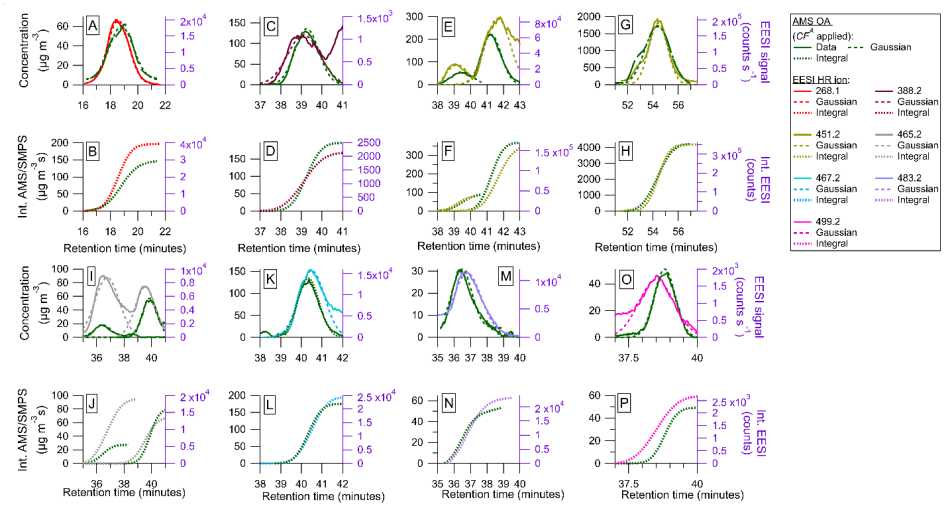

Formatted: Font: Bold

Formatted Table

Commented [P11]: Deleted image, reformatted

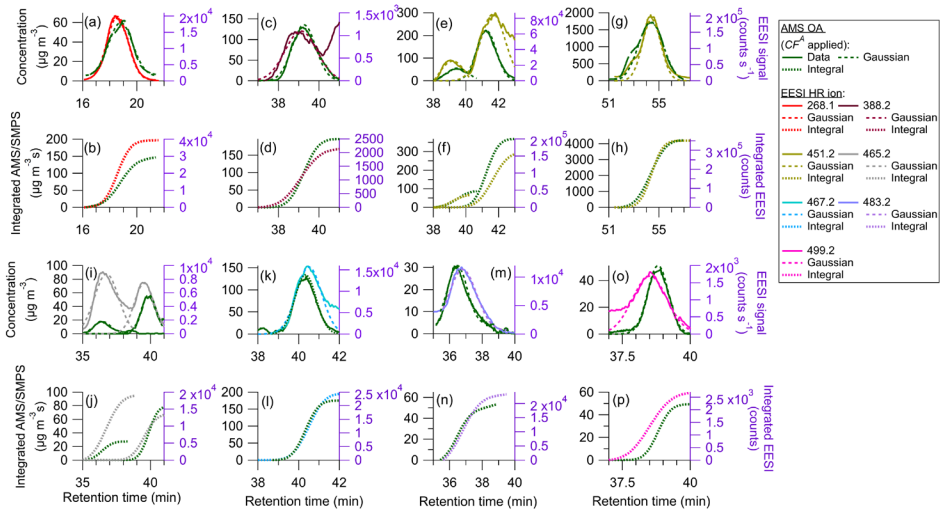

Figure S13. (a) *m/z*= 268.1 Gaussians, (b) integrals; (c) *m/z*= 388.2 Gaussians, (d) integrals; (e) one peak for *m/z*= 451.2 Gaussians, (f) integrals; (g) one peak for *m/z*= 451.2 Gaussians, (h) integrals; (i) *m/z*= 465.2 Gaussians, (j) integrals; (k) *m/z*= 467.2 Gaussians, (l) integrals; (m) one peak for *m/z*=4 483.2 Gaussians, (n) integrals; (o) *m/z*= 499.2 Gaussians, (p) integrals. For the EESI HR ions, the total mass (~~Org~~OA + NO_3) was used in the denominator.

Formatted: Font: 10 pt

Formatted: Font: 10 pt

Not every peak observed in Claflin and Ziemann (2018) was identified here, which is likely due to lack of EESI sensitivity to some species and potential decomposition of SOA products (specifically for the trimer identified in Claflin and Ziemann (2018)). In contrast, some EESI HR ions that do not correspond to peaks identified in Claflin and Ziemann (2018) were detected here, but structures for those species are unknown. All identified individual peaks are shown in Fig. S13. As described in Sect. 2.7, CF_x^E was determined either using the measured SMPS mass or the total AMS mass (OA~~Org~~ + NO_3). Fig. S13 shows the AMS OA mass, which was separated by PMF. As shown in Fig. S3, the NO_3 contribution to the total mass was ~ 5 %. This contribution was added to the denominator to calculate CF_x^E which are reported in table 2 in the main text.

References

Boyd, C. M., J. Sanchez, L. Xu, a. J. Eugene, T. Nah, W. Y. Tuet, M. I. Guzman, and N. L. Ng. 2015. "Secondary Organic Aerosol Formation from the β-Pinene+NO_3 System: Effect of Humidity and Peroxy Radical Fate." *Atmospheric Chemistry and Physics* 15 (13): 7497–7522.

Claflin, M. S. and Ziemann, P. J.: Identification and Quantitation of Aerosol Products of the Reaction of β-Pinene with NO3 Radicals and Implications for Gas- and Particle-Phase Reaction Mechanisms, J. Phys. Chem. A, 122(14), 3640–3652, doi:10.1021/acs.jpca.8b00692, 2018.

Collins, D. R., Flagan, R. C. and Seinfeld, J. H.: Improved inversion of scanning DMA data, Aerosol Sci. Technol., 36(1), 1–9, doi:10.1080/027868202753339032, 2002.

DeCarlo, P. F., Dunlea, E. J., Kimmel, J. R., Aiken, A. C., Sueper, D., Crounse, J., Wennberg, P. O., Emmons, L., Shinozuka, Y., Clarke, A. and Others: Fast airborne aerosol size and chemistry measurements above Mexico City and Central Mexico during the MILAGRO campaign, 1foldr Import 2019-10-08 Batch 1 [online] Available from: https://oaktrust.library.tamu.edu/bitstream/handle/1969.1/178622/document-2.pdf?sequence=2, 2008.

Huffman, J. A., Jayne, J. T., Drewnick, F., Aiken, A. C., Onasch, T., Worsnop, D. R. and Jimenez, J. L.: Design, Modeling, Optimization, and Experimental Tests of a Particle Beam Width Probe for the Aerodyne Aerosol Mass Spectrometer, Aerosol Sci. Technol., 39(12), 1143–1163, doi:10.1080/02786820500423782, 2005.

Jayne, J. T., Leard, D. C., Zhang, X., Davidovits, P., Smith, K. A., Kolb, C. E. and Worsnop, D. R.: Development of an Aerosol Mass Spectrometer for Size and Composition Analysis of Submicron Particles, Aerosol Sci. Technol., 33(1-2), 49–70, doi:10.1080/027868200410840, 2000.

Jeong, C.-H. and Evans, G. J.: Inter-Comparison of a Fast Mobility Particle Sizer and a Scanning Mobility Particle Sizer Incorporating an Ultrafine Water-Based Condensation Particle Counter, Aerosol Sci. Technol., 43(4), 364–373, doi:10.1080/02786820802662939, 2009.

Krechmer, J. E., Day, D. A., Ziemann, P. J. and Jimenez, J. L.: Direct Measurements of Gas/Particle Partitioning and Mass Accommodation Coefficients in Environmental Chambers, Environ. Sci. Technol., 51(20), 11867–11875, doi:10.1021/acs.est.7b02144, 2017.

Malloy, Q. G. J., Nakao, S., Qi, L., Austin, R., Stothers, C., Hagino, H. and Cocker, D. R.: Real-Time Aerosol Density Determination Utilizing a Modified Scanning Mobility Particle Sizer—Aerosol Particle Mass Analyzer System, Aerosol Sci. Technol., 43(7), 673–678, doi:10.1080/02786820902832960, 2009.

McMurry, P. H.: A review of atmospheric aerosol measurements, Atmos. Environ., 34(12), 1959–1999, doi:10.1016/S1352-2310(99)00455-0, 2000.

Pagonis, D., Campuzano-Jost, P., Guo, H., Day, D. A., Schueneman, M. K., Brown, W. L., Nault, B. A., Stark, H., Siemens, K., Laskin, A., Piel, F., Tomsche, L., Wisthaler, A., Coggon, M. M., Gkatzelis, G. I., Halliday, H. S., Krechmer, J. E., Moore, R. H., Thomson, D. S., Warneke, C., Wiggins, E. B. and Jimenez, J. L.: Airborne extractive electrospray mass spectrometry measurements of the chemical composition of organic aerosol, Atmospheric Measurement Techniques, 14(2), 1545–1559, doi:10.5194/amt-14-1545-2021, 2021.

Russell, L. M., Flagan, R. C. and Seinfeld, J. H.: Asymmetric Instrument Response Resulting from Mixing Effects in Accelerated DMA-CPC Measurements, Aerosol Sci. Technol., 23(4), 491–509, doi:10.1080/02786829508965332, 1995.

Sinclair, D. and La Mer, V. K.: Light scattering as a measure of particle size in aerosols; the production of monodisperse aerosols, Chem. Rev., 44(2), 245–267, doi:10.1021/cr60138a001, 1949.

Sioutas, C.: Evaluation of the Measurement Performance of the Scanning Mobility Particle Sizer and Aerodynamic Particle Sizer, Aerosol Sci. Technol., 30(1), 84–92, doi:10.1080/027868299304903, 1999.

Ulbrich, I. M., Canagaratna, M. R., Zhang, Q., Worsnop, D. R. and Jimenez, J. L.: Interpretation of organic components from positive matrix factorization of aerosol mass spectrometric data, Atmospheric Chemistry & Physics, 9(9) [online] Available from: https://d-nb.info/114970523X/34, 2009.

Wang, S. C. and Flagan, R. C.: Scanning Electrical Mobility Spectrometer, Aerosol Sci. Technol., 13(2), 230–240, doi:10.1080/02786829008959441, 1990.

Formatted: Font: 10 pt

Formatted: Font: 10 pt

Formatted: Font: 10 pt

Formatted: Font: 10 pt

Formatted: Font: 10 pt

Formatted: Font: 10 pt

Formatted: Font: Font color: Black